One-loop corrections for WW to HH in Higgs EFT with the electroweak chiral Lagrangian

M. J. Herrero[1,*] and R. A. Morales[2,†]

[1]*Departamento de Física Teórica and Instituto de Física Teórica, IFT-UAM/CSIC, Universidad Autónoma de Madrid, Cantoblanco, 28049 Madrid, Spain*

[2]*IFLP, CONICET—Departamento de Física, Universidad Nacional de La Plata, C.C. 67, 1900 La Plata, Argentina*

(Received 22 August 2022; accepted 21 September 2022; published 28 October 2022)

In this work, we present the computation of the one-loop electroweak radiative corrections to the scattering process $WW \to HH$ within the context of the Higgs Effective Field Theory (HEFT). We assume that the fermionic interactions are like in the Standard Model, whereas the beyond Standard Model interactions in the bosonic sector are given by the electroweak chiral Lagrangian (EChL). The computation of the one-loop amplitude and the renormalization program is performed in terms of the involved one-particle-irreducible (1PI) functions and using R_ξ covariant gauges. The renormalization of 1PI functions at arbitrary external momenta is a more ambitious program than just renormalizing the amplitude with on-shell external legs, and it has the advantage that they can be used in several scattering amplitudes. In fact, we use here some of the 1PI functions already computed in our previous work (devoted to $WZ \to WZ$). We will complement them here with the computation of the new 1PI functions required for $WW \to HH$. From this renormalization procedure, we will also derive the full set of renormalized coefficients of the EChL that are relevant for this scattering process. In the last part, we will present the numerical results for the EChL predictions of the one-loop level cross section, $\sigma(WW \to HH)|_{\text{1-loop}}$, as a function of the center-of-mass energy, showing the relative size of the one-loop radiative corrections with respect to the tree-level prediction in terms of the EChL coefficients. The results of the one-loop corrections to $WW \to HH$ for the SM case will be also presented, for comparison with the EChL case, following the same computational method—i.e., by means of the renormalization of 1PI functions.

DOI: 10.1103/PhysRevD.106.073008

I. INTRODUCTION

The use of effective field theories (EFTs) to study the phenomenological implications of anomalous Higgs couplings beyond the Standard Model (SM) of particle physics is nowadays a very common strategy, widely employed, to test at colliders the new Higgs physics implied by those anomalous couplings in a model-independent way—namely, without assuming a particular model of physics beyond the Standard Model (BSM). The information of the anomalous Higgs couplings is encoded in a set of effective operators, built with the SM fields and with the unique requirement of being invariant under the SM gauge symmetry, $SU(3) \times SU(2) \times U(1)$. The coefficients in front of these operators (usually called Wilson coefficients) are generically unknown and encode the information of the particular underlying fundamental theory that generates such EFTs at low energies when the new heavy modes of this theory are integrated out. Depending on the kind of dynamics involved in the fundamental theory, it is more appropriate the use of one EFT or another. Usually, the so-called SMEFT (Standard Model effective theory) is more appropriate to describe the low-energy behavior of weakly interacting dynamics, whereas the so-called HEFT (Higgs effective field theory) is more appropriate to describe strongly interacting underlying dynamics (for reviews, see, for instance, Refs. [1,2]). Here we choose this second case, the HEFT, and focus on the bosonic sector which is described in terms of the so-called electroweak chiral Lagrangian (EChL). The fermionic sector will be assumed to be as in the SM, so that no BSM interactions or effective operators are considered in the fermionic sector of the HEFT.

Our main goal here is to determine, within this EChL context, the size of the one-loop electroweak (EW) radiative corrections for the subprocess at colliders, $W^+W^- \to HH$,

*maria.herrero@uam.es

†roberto.morales@fisica.unlp.edu.ar

where two Higgs bosons are produced from the scattering of two W gauge bosons which are radiated from the initial colliding particles (also called WW fusion in the literature). From now on, for brevity, we omit the explicit charges of the W bosons. This WW scattering subprocess is known to be relevant for both types of colliders, e^+e^- and pp, with energies at the TeV domain. We also wish to compare in this work these EW radiative corrections in the EChL context with the corresponding ones of $WW \to HH$ within the SM context; thus, we perform here the two computations in parallel. Our calculations of the amplitudes and corresponding cross sections in both cases, the EChL and the SM, are full bosonic one-loop computations, including all kinds of diagrams in the loops, and are valid for physical W and H particles in the external legs, with all possible polarizations for the W gauge bosons, longitudinal and transverse. That means that we do not make any approximation for the external legs, and we do not use the equivalence theorem (ET) which replaces the external W_L's with the corresponding Goldstone bosons (GBs) and is valid only at high energies, $\sqrt{s} \gg m_{\mathrm{W}}$. Our computation of the radiative corrections within the HEFT is therefore valid at all energies, from the low energies just above the two-Higgs-boson threshold production, $2m_{\mathrm{H}} \sim 250$ GeV, up to the typical EFT scale which, in the EChL framework, is set by $4\pi v \sim 3$ TeV with $v = 246$ GeV.

Regarding the technicalities involved in the present computation, we follow closely our previous work in Ref. [3], which was addressed to the case of $WZ \to WZ$ scattering. Concretely, we follow the standard Feynman diagrammatic approach and describe the full renormalization program also in terms of one-loop Feynman diagrams. We organize this computation in terms of the involved one-particle-irreducible (1PI) Green's functions, with two, three, and four external legs, and perform the renormalization program of these Green's functions in covariant gauges. As we showed in our previous work [3], the renormalization of the EChL coefficients must be gauge invariant and therefore independent of the ξ parameter of the R_ξ covariant gauges. This is an important point of performing the analytical computation of the amplitude in covariant gauges. Regarding the numerical evaluations for the $WW \to HH$ scattering, we will choose here in particular the Feynman–'t Hooft gauge with $\xi = 1$. The renormalization conditions are also fixed here as in Ref. [3], using the on-shell scheme for the EW parameters, like the boson masses m_{W}, m_{Z}, m_{H} and gauge couplings, and the $\overline{\mathrm{MS}}$ scheme for the EChL coefficients. Our work presented here of the full one-loop corrections for $WW \to HH$ in the EChL is the most complete one in the literature and improves the previous related works in the literature in various aspects. The first computation of $WW \to HH$ in Ref. [4] was performed just for the case with external longitudinal W bosons, which were replaced by external GBs by using the ET, and includes only scalar particles both in the external legs and in the loops, working always with massless GBs. A more recent computation of the one-loop radiative corrections for $WW \to HH$ in the EChL context, in Ref. [5], also refers to the case of longitudinal W's and also uses the ET to replace the external W_L with the GBs, which are taken to be massless. They consider all kinds of loops for the GB scattering and compute them in the Landau gauge. They make the additional approximation of taking as equal the W and Z boson masses (called the isospin limit in the literature). Our best improvement with respect to these works is that we do not use the ET—i.e., we work with external gauge bosons instead of GBs, we do not take equal masses for W and Z, and we do not take massless GBs, since we work in the Feynman–'t Hooft gauge. Consequently, the sets of Feynman one-loop diagrams considered here and in Refs. [4,5] are also different. Another important aspect that we cover in a different way than in those references is the renormalization program, which we implement here in terms of general renormalized Green's functions, with generic external momenta, in contrast to Refs. [4,5], which apply the renormalization program directly to the on-shell scattering amplitude. The advantage of doing renormalization at the more general off-shell Green's function level, is that these same renormalized functions can be used as well for the computation of radiative corrections in other observables. For instance, we have used the same renormalized vertex function WWH here for $WW \to HH$ as in our previous computation in Ref. [3] for $WZ \to WZ$. The difference is just in the particular setting of the external legs' momenta of the vertex function, which must be done properly for each case. On the other hand, the renormalization program using 1PI Green's functions instead of just on-shell amplitudes requires the renormalization of a larger set of EChL coefficients. It is, therefore, also more complete in this sense. Due to the relevance of this latter issue, we will devote some part of the present work to the comparison of our results on the renormalization of the EChL coefficients with some related previous results [4–7].

The paper is organized as follows: In Sec. II, we briefly describe the main features of the EChL with R_ξ gauge fixing and set the relevant operators for the $WW \to HH$ scattering process. The diagrammatic computation by means of the 1PI functions is presented in Sec. III. Section IV is devoted to the renormalization program, including the prescriptions for regularization and renormalization assumed and the summary of all the divergent counterterms. The numerical predictions for this observable within the EChL and the SM are presented and discussed in Sec. V. Finally, we conclude in Sec. VI.

II. RELEVANT PART OF THE ELECTROWEAK CHIRAL LAGRANGIAN

In this section, we introduce the part of the bosonic EChL that is needed for the present computation of the EW

radiative corrections of the $WW \to HH$ scattering, and we provide some necessary notation. In the EChL context, the active fields are the EW gauge bosons, B_μ and W^a_μ $(a = 1, 2, 3)$; their corresponding GBs π^a $(a = 1, 2, 3)$; and the Higgs boson H. The unique requirement for the building of the EChL is invariance under the EW gauge transformations, $SU(2)_L \times U(1)_Y$. On the other hand, the scalar sector of the EChL has an additional invariance under the EW chiral transformation, $SU(2)_L \times SU(2)_R$. Under this EW chiral transformation, the GBs transform nonlinearly. This peculiarity implies multiple GB interactions among themselves and also with the other fields. The Higgs boson field, in contrast, is invariant under all transformations. Usually the GBs are introduced in a nonlinear representation via the exponential parametrization, by means of the matrix U, which transforms linearly under the EW chiral transformations:

$$U(\pi^a) = e^{i\pi^a \tau^a / v}, \tag{2.1}$$

where τ^a, $a = 1, 2, 3$ are the Pauli matrices and $v = 246$ GeV. On the other hand, the Higgs field is a singlet of the EW chiral symmetry and the EW gauge symmetry. Hence, the interactions of H are introduced via generic polynomials, since there are no limitations from symmetry arguments on the implementation of this field and its interactions with itself and with the other fields, in contrast to linear EFTs such as the SMEFT. Finally, the EW gauge bosons are introduced by the gauge invariance principle. Thus, they appear in the following pieces of the EChL:

$$\begin{aligned}
&\hat{B}_\mu = g' B_\mu \tau^3/2, \qquad \hat{B}_{\mu\nu} = \partial_\mu \hat{B}_\nu - \partial_\nu \hat{B}_\mu, \\
&\hat{W}_\mu = g W^a_\mu \tau^a/2, \qquad \hat{W}_{\mu\nu} = \partial_\mu \hat{W}_\nu - \partial_\nu \hat{W}_\mu + i[\hat{W}_\mu, \hat{W}_\nu], \\
&D_\mu U = \partial_\mu U + i\hat{W}_\mu U - iU\hat{B}_\mu, \qquad \mathcal{V}_\mu = (D_\mu U)U^\dagger, \\
&\mathcal{D}_\mu O = \partial_\mu O + i[\hat{W}_\mu, O].
\end{aligned} \tag{2.2}$$

As usual, the chiral counting arranges the effective operators in the EChL into terms with increasing chiral dimension. The most relevant ones are the leading-order Lagrangian, with chiral dimension two, $\mathcal{L}_2$, and the next-to-leading-order one with chiral dimension four, $\mathcal{L}_4$. The relevant EChL for the present computation can then be summarized as follows:

$$\mathcal{L}_{\rm EChL} = \mathcal{L}_2 + \mathcal{L}_4. \tag{2.3}$$

In this chiral dimension counting, it is important to keep in mind that all derivatives and masses count as momentum—namely, ∂_μ, $m_{\rm W}$, $m_{\rm Z}$, $m_{\rm H}$, gv, $g'v$, $\lambda v \sim \mathcal{O}(p)$.

First, the leading-order Lagrangian $\mathcal{L}_2$ is given by

$$\begin{aligned}
\mathcal{L}_2 = {} & \frac{v^2}{4}\left(1 + 2a\frac{H}{v} + b\left(\frac{H}{v}\right)^2 + \cdots\right)\mathrm{Tr}[D_\mu U^\dagger D^\mu U] \\
& + \frac{1}{2}\partial_\mu H \partial^\mu H - V(H) - \frac{1}{2g^2}\mathrm{Tr}[\hat{W}_{\mu\nu}\hat{W}^{\mu\nu}] \\
& - \frac{1}{2g'^2}\mathrm{Tr}[\hat{B}_{\mu\nu}\hat{B}^{\mu\nu}] + \mathcal{L}_{GF} + \mathcal{L}_{FP}.
\end{aligned} \tag{2.4}$$

Here, $V(H)$ is the Higgs potential, and $\mathcal{L}_{\rm GF}$ and $\mathcal{L}_{\rm FP}$ are the gauge-fixing Lagrangian and Fadeev-Popov Lagrangian, respectively. From now on, the dots in the presentation of the relevant pieces in the EChL stand for terms that do not enter into our process of interest, $WW \to HH$, neither at tree level nor at one-loop level; thus, we omit them. The Higgs potential in $\mathcal{L}_2$ is given by

$$\begin{aligned}
V(H) = {} & (-\mu^2 + \lambda v^2) v H + \frac{1}{2}(-\mu^2 + 3\lambda v^2) H^2 \\
& + \kappa_3 \lambda v H^3 + \kappa_4 \frac{\lambda}{4} H^4.
\end{aligned} \tag{2.5}$$

For the posterior discussion on renormalization in this EChL context, it is convenient to define $m^2_{\rm H} = -\mu^2 + 3\lambda v^2$; then, we can eliminate the μ^2 parameter in terms of $m^2_{\rm H}$. In this case, the linear term (Higgs tadpole) can be simply written as

$$T = (m^2_{\rm H} - 2\lambda v^2) v, \tag{2.6}$$

and the minimum of the potential, corresponding to a vanishing tadpole, sets $m^2_{\rm H} = 2\lambda v^2$.

Here, we quantize the EChL as in our previous work [3]—i.e., using the linear covariant R_ξ gauges [8] with the gauge-fixing Lagrangian given by

$$\mathcal{L}_{\rm GF} = -F_+ F_- - \frac{1}{2}F_Z^2 - \frac{1}{2}F_A^2, \tag{2.7}$$

and the gauge-fixing functions given by

$$\begin{aligned}
&F_\pm = \frac{1}{\sqrt{\xi}}(\partial^\mu W^\pm_\mu - \xi m_{\rm W} \pi^\pm), \\
&F_Z = \frac{1}{\sqrt{\xi}}(\partial^\mu Z_\mu - \xi m_{\rm Z} \pi^3), \qquad F_A = \frac{1}{\sqrt{\xi}}(\partial^\mu A_\mu).
\end{aligned} \tag{2.8}$$

Here, ξ is the generic gauge-fixing parameter of the R_ξ gauges. Some comments about the ξ dependence are worth adding here. Notice that in our renormalization program, we demand the renormalization of all the 1PI functions involved at arbitrary momentum for the external legs, and not just the finiteness of the one-loop scattering amplitude. Thus, in order to demonstrate explicitly the gauge invariance of the renormalized EChL coefficients—i.e., to check that these are ξ independent—the computation of the loop diagrams involved in the 1PI functions should be performed for an arbitrary ξ parameter, as was done in our

previous work [3] devoted to $WZ \to WZ$ scattering. All the final scattering amplitudes with external on-shell particles are, of course, finite and gauge invariant, but the involved 1PI functions are ξ dependent, so the cancellation of the ξ dependence in the final one-loop amplitude is an excellent check of the computation. In the present paper, for all the numerical estimates of $WW \to HH$, we will choose in particular the Feynman–'t Hooft gauge, and accordingly, for definiteness, we set $\xi = 1$ in the presentation of all our results.

From this previous R_ξ gauge-fixing Lagrangian, one derives as usual the corresponding Faddeev-Popov Lagrangian [9], given by

$$\mathcal{L}_{\rm FP} = \sum_{i,j=+,-,Z,A} \bar{c}^i \frac{\delta F_i}{\delta \alpha_j} c^j, \tag{2.9}$$

where c^j are the ghost fields and α_j ($j = +, -, Z, A$) are the corresponding gauge transformation parameters under the local transformations $SU(2)_L \times U(1)_Y$ given by $L = e^{ig\vec{\tau}\cdot\vec{\alpha}_L(x)/2}$ and $R = e^{ig'\tau^3\alpha_Y(x)/2}$.

Formally, the expressions in Eqs. (2.7)–(2.9) and the gauge bosons' field transformations are the same as in the SM. However, the scalar transformations in this nonlinear EFT differ from the corresponding ones in the SM. This particularity yields to the absence of interactions among the Higgs boson and ghost fields, and the presence of new interactions with multiple GBs and two ghost fields.

Second, the relevant chiral dimension-four Lagrangian for the computation of all the one-loop 1PI functions involved in the $WW \to HH$ scattering amplitude is given by

$$\begin{aligned}
\mathcal{L}_4 = & -a_{ddVV1}\frac{\partial^\mu H \partial^\nu H}{v^2}\mathrm{Tr}[\mathcal{V}_\mu \mathcal{V}_\nu] - a_{ddVV2}\frac{\partial^\mu H \partial_\mu H}{v^2}\mathrm{Tr}[\mathcal{V}^\nu \mathcal{V}_\nu] \\
& + \left(a_{11} + a_{H11}\frac{H}{v} + a_{HH11}\frac{H^2}{v^2}\right)\mathrm{Tr}[\mathcal{D}_\mu \mathcal{V}^\mu \mathcal{D}_\nu \mathcal{V}^\nu] - \frac{m_{\rm H}^2}{4}\left(2a_{HVV}\frac{H}{v} + a_{HHVV}\frac{H^2}{v^2}\right)\mathrm{Tr}[\mathcal{V}^\mu \mathcal{V}_\mu] \\
& - \left(a_{HWW}\frac{H}{v} + a_{HHWW}\frac{H^2}{v^2}\right)\mathrm{Tr}[\hat{W}_{\mu\nu}\hat{W}^{\mu\nu}] + i\left(a_{d2} + a_{Hd2}\frac{H}{v}\right)\frac{\partial^\nu H}{v}\mathrm{Tr}[\hat{W}_{\mu\nu}\mathcal{V}^\mu] \\
& + \left(a_{\Box VV} + a_{H\Box VV}\frac{H}{v}\right)\frac{\Box H}{v}\mathrm{Tr}[\mathcal{V}_\mu \mathcal{V}^\mu] + \left(a_{d3} + a_{Hd3}\frac{H}{v}\right)\frac{\partial^\nu H}{v}\mathrm{Tr}[\mathcal{V}_\nu \mathcal{D}_\mu \mathcal{V}^\mu] \\
& + \left(a_{\Box\Box} + a_{H\Box\Box}\frac{H}{v}\right)\frac{\Box H \Box H}{v^2} + a_{dd\Box}\frac{\partial^\mu H \partial_\mu H \Box H}{v^3} \\
& + \left(a_{Hdd}\frac{m_{\rm H}^2}{v^2} + a_{ddW}\frac{m_{\rm W}^2}{v^2} + a_{ddZ}\frac{m_{\rm Z}^2}{v^2}\right)\frac{H}{v}\partial^\mu H \partial_\mu H.
\end{aligned} \tag{2.10}$$

These relevant effective operators are taken from the full HEFT Lagrangian in Refs. [6,10], but we use here a different notation for the EChL coefficients in $\mathcal{L}_4$, which are referred to here generically as a_i's. The correspondence among the two sets of coefficients, the a_i's here and the coefficients in Refs. [6,10], can be summarized, in short, by $a_{ddVV1} \leftrightarrow c_8$, $a_{ddVV2} \leftrightarrow c_{20}$, $a_{11} \leftrightarrow c_9$, $a_{HWW} \leftrightarrow a_W$, $a_{HHWW} \leftrightarrow b_W$, $a_{d2} \leftrightarrow c_5$, $a_{Hd2} \leftrightarrow a_5$, $a_{\Box VV} \leftrightarrow c_7$, $a_{H\Box VV} \leftrightarrow a_7$, $a_{d3} \leftrightarrow c_{10}$, $a_{Hd3} \leftrightarrow a_{10}$, $a_{\Box\Box} \leftrightarrow c_{\Box H}$, $a_{H\Box\Box} \leftrightarrow a_{\Box H}$, $a_{dd\Box} \leftrightarrow c_{\Delta H}$, $a_{HVV} \leftrightarrow a_C$, and $a_{HHVV} \leftrightarrow b_C$.

It is worth noticing that, in contrast to our one-loop computation here, for a tree-level computation of the scattering amplitude (see, for instance, Ref. [11]), the previous set of operators in $\mathcal{L}_4$ can be reduced to a smaller set by the use of the equations of motion (EOMs). Concretely, one may use the following EOMs involving the pieces $\Box H$, $\mathcal{D}_\mu \mathcal{V}^\mu$ and $\mathcal{F}(H) = 1 + 2a\frac{H}{v} + b(\frac{H}{v})^2$:

$$\begin{aligned}
\Box H &= -\frac{\delta V(H)}{\delta H} - \frac{v^2}{4}\frac{\mathcal{F}(H)}{\delta H}\mathrm{Tr}[\mathcal{V}^\mu \mathcal{V}_\mu] \Rightarrow \\
\Rightarrow \Box H &= -m_{\rm H}^2 H - \frac{3}{2}\kappa_3 m_{\rm H}^2 \frac{H^2}{v} - \frac{a}{2}v\mathrm{Tr}[\mathcal{V}^\mu \mathcal{V}_\mu] \\
& \quad - \frac{b}{2}H\mathrm{Tr}[\mathcal{V}^\mu \mathcal{V}_\mu], \\
\mathrm{Tr}[\tau^j \mathcal{D}_\mu \mathcal{V}^\mu]\mathcal{F}(H) &= -\mathrm{Tr}[\tau^j \mathcal{V}^\mu]\partial_\mu \mathcal{F}(H) \Rightarrow \\
\Rightarrow \mathrm{Tr}[\tau^j \mathcal{D}_\mu \mathcal{V}^\mu] &= -\mathrm{Tr}[\tau^j \mathcal{V}^\mu]\frac{2a}{v}\partial_\mu H.
\end{aligned} \tag{2.11}$$

Then, one may eliminate the terms in $\mathcal{L}_4$ involving these two pieces by rewriting them in terms of the other effective operators. This reduces in practice the number of effective operators in $\mathcal{L}_4$ as follows:

$$\begin{aligned}\mathcal{L}_4^{+\mathrm{EOMs}} = &-(a_{dd\mathcal{V}\mathcal{V}1} - 4a^2 a_{11} + 2a a_{d3})\frac{\partial^\mu H \partial^\nu H}{v^2}\mathrm{Tr}[\mathcal{V}_\mu \mathcal{V}_\nu] - \left(a_{dd\mathcal{V}\mathcal{V}2} + \frac{a}{2}a_{dd\Box}\right)\frac{\partial^\mu H \partial_\mu H}{v^2}\mathrm{Tr}[\mathcal{V}^\nu \mathcal{V}_\nu] \\ &- \frac{m_{\mathrm{H}}^2}{2}(a_{H\mathcal{V}\mathcal{V}} - 2a_{\Box\mathcal{V}\mathcal{V}} + 2a a_{\Box\Box})\frac{H}{v}\mathrm{Tr}[\mathcal{V}^\mu \mathcal{V}_\mu] \\ &- \frac{m_{\mathrm{H}}^2}{4}(a_{HH\mathcal{V}\mathcal{V}} - 6\kappa_3 a_{\Box\mathcal{V}\mathcal{V}} - 4a_{H\Box\mathcal{V}\mathcal{V}} + 4b a_{\Box\Box} + 6\kappa_3 a a_{\Box\Box} + 4a a_{H\Box\Box})\frac{H^2}{v^2}\mathrm{Tr}[\mathcal{V}^\mu \mathcal{V}_\mu] \\ &+ (a_{Hdd} - a_{dd\Box})\frac{m_{\mathrm{H}}^2}{v^2}\frac{H}{v}\partial^\mu H \partial_\mu H + \left(a_{ddW}\frac{m_{\mathrm{W}}^2}{v^2} + a_{ddZ}\frac{m_{\mathrm{Z}}^2}{v^2}\right)\frac{H}{v}\partial^\mu H \partial_\mu H \\ &- \left(a_{HWW}\frac{H}{v} + a_{HHWW}\frac{H^2}{v^2}\right)\mathrm{Tr}[\hat{W}_{\mu\nu}\hat{W}^{\mu\nu}] + i\left(a_{d2} + a_{Hd2}\frac{H}{v}\right)\frac{\partial^\nu H}{v}\mathrm{Tr}[\hat{W}_{\mu\nu}\mathcal{V}^\mu]. \end{aligned} \tag{2.12}$$

In this reduced Lagrangian, $a_{dd\mathcal{V}\mathcal{V}1}$, a_{11}, and a_{d3} have been grouped together in the first operator, $a_{dd\mathcal{V}\mathcal{V}2}$ and $a_{dd\Box}$ in the second operator, etc. We then redefine these combinations of coefficients as follows:

$$\begin{aligned}\eta = \tilde{a}_{dd\mathcal{V}\mathcal{V}1} &\equiv a_{dd\mathcal{V}\mathcal{V}1} - 4a^2 a_{11} + 2a a_{d3}, \\ \delta = \tilde{a}_{dd\mathcal{V}\mathcal{V}2} &\equiv a_{dd\mathcal{V}\mathcal{V}2} + \frac{a}{2}a_{dd\Box}, \\ \tilde{a}_{H\mathcal{V}\mathcal{V}} &\equiv a_{H\mathcal{V}\mathcal{V}} - 2a_{\Box\mathcal{V}\mathcal{V}} + 2a a_{\Box\Box}, \\ \tilde{a}_{HH\mathcal{V}\mathcal{V}} &\equiv a_{HH\mathcal{V}\mathcal{V}} - 6\kappa_3 a_{\Box\mathcal{V}\mathcal{V}} - 4a_{H\Box\mathcal{V}\mathcal{V}} + 4b a_{\Box\Box} + 6\kappa_3 a a_{\Box\Box} + 4a a_{H\Box\Box}, \\ \tilde{a}_{Hdd} &\equiv a_{Hdd} - a_{dd\Box}. \end{aligned} \tag{2.13}$$

Notice that in the two first coefficients, we have also used the alternative notation given by η and δ, which is the one frequently used in some related literature. In particular, the contributions to the scattering amplitude $WW \to HH$ of these two first operators in the above list with η and δ coefficients were studied first in Refs. [4,5]. We will compare our results with these and more references in later sections. Notice also that some coefficients, like a_{H11}, a_{HH11}, and a_{Hd3}, have disappeared in Eq. (2.12) since, after the use of the EOMs, they contribute to effective operators with at least three Higgs bosons which do not enter into the process of our interest here.

The main consequence of using the EOMs when computing the scattering amplitude is that these combinations of the EChL coefficients are the ones appearing precisely in the on-shell scattering amplitudes. On the other hand, this means that only these combinations of coefficients are the ones that are really testable at colliders via this particular $WW \to HH$ scattering. In particular, only η and δ in Eq. (2.13) and not the separate coefficients, $a_{dd\mathcal{V}\mathcal{V}1}$, a_{11}, a_{d3}, $a_{dd\mathcal{V}\mathcal{V}2}$, and $a_{dd\Box}$, are the appropriate parameters for a phenomenological analysis of this scattering $WW \to HH$ process, and similarly for the other combinations appearing in Eq. (2.12). However, for our most ambitious computation and renormalization program, where the finite renormalized one-loop scattering amplitude is obtained in terms of finite renormalized one-loop 1PI functions, this reduced Lagrangian is not sufficient, and we must use the full Lagrangian in Eq. (2.10). As we will see in the following sections, this full Lagrangian provides not only a finite one-loop amplitude with on-shell external particles but also finite one-loop 1PI functions with arbitrary external momenta (generically off shell). This renormalization program in terms of one-loop 1PI functions is also relevant for the check of the gauge invariance of the final one-loop amplitude, and to demonstrate the gauge invariance of the renormalized EChL coefficients. The great advantage of using this procedure by means of the 1PI functions to compute the radiative corrections in scattering amplitudes is that the same 1PI one-loop renormalized functions, once computed at arbitrary external momenta, can be used for several processes, by just adjusting the external momenta to those of that particular process, including the proper on-shell setting for the external legs when needed. For instance, the one-loop 1PI function $\hat{\Gamma}_{HWW}$ can be used for both $WW \to HH$ and $WZ \to WZ$, the one-loop 1PI function $\hat{\Gamma}_{HHH}$ can be used for both $WW \to HH$ and $HH \to HH$, and similarly with other processes. Therefore, our renormalization program based on 1PI functions is more powerful than just renormalizing concrete scattering amplitudes.

Finally, to end this section, we remind the reader that in order to reach the SM tree-level vertices from the above presented EChL, one has to set the EFT coefficients to the following reference values: (i) the coefficients in $\mathcal{L}_2$, a, b, κ_3, and κ_4 should be set to 1, and (ii) all the a_i's coefficients in $\mathcal{L}_4$ should be set to zero. Accordingly, the new BSM physics encoded in the EChL is parametrized in terms of the departures from these reference parameter values. The corresponding derived Feynman rules (FRs) from this

EChL that are needed for the present computation, together with the corresponding FRs within the SM, were provided in our previous work, concretely in Appendix A of Ref. [3], so we do not repeat them here.

III. DIAGRAMMATIC COMPUTATION USING 1PI GREEN'S FUNCTIONS

In this section, we present our procedure for the computation of the radiative corrections to the amplitude $\mathcal{A}(WW \to HH)$ by means of the 1PI Green's functions. We apply this procedure to both cases, the EChL and the SM.

Within the EChL formalism, the full one-loop scattering amplitude can be split into two parts corresponding to the leading-order (LO), $\mathcal{O}(p^2)$, and the next-to-leading-order contributions (NLO), $\mathcal{O}(p^4)$, which are denoted as $\mathcal{A}^{(0)}$ and $\mathcal{A}^{(1)}$, respectively, yielding to

$$\begin{aligned}\mathcal{A}^{\mathrm{EChL_{Full}}} &\equiv \mathcal{A}(WW \to HH)^{\mathrm{EChL}} \\ &= \mathcal{A}^{(0)}(WW \to HH) \\ &\quad + \mathcal{A}^{(1)}(WW \to HH). \end{aligned} \tag{3.1}$$

In this EChL context, the LO amplitude comes from $\mathcal{L}_2$ at the tree level, and the NLO amplitude receives typically two contributions. One contribution comes from $\mathcal{L}_4$ at the tree level, and the other comes from the loops computed with $\mathcal{L}_2$. Thus, these LO and NLO contributions are written generically as

$$\mathcal{A}^{(0)}(WW \to HH) \equiv \mathcal{A}^{\mathrm{EChL}^{(2)}_{\mathrm{Tree}}}, \tag{3.2}$$

$$\mathcal{A}^{(1)}(WW \to HH) \equiv \mathcal{A}^{\mathrm{EChL}^{(4)}_{\mathrm{Tree}}} + \mathcal{A}^{\mathrm{EChL}^{(2)}_{\mathrm{Loop}}}. \tag{3.3}$$

The one-loop amplitude in the EChL can also be written in an alternative way, accounting for the quantum corrections expansion—i.e., in powers of $\hbar$. Then, the full one-loop amplitude is written as

$$\mathcal{A}^{\mathrm{EChL_{Full}}} = \mathcal{A}^{\mathrm{EChL}^{(2+4)}_{\mathrm{Tree}}} + \mathcal{A}^{\mathrm{EChL}^{(2)}_{\mathrm{Loop}}}, \tag{3.4}$$

where the tree level amplitude, $\mathcal{O}(\hbar^0)$, has contributions from both $\mathcal{L}_2$ and $\mathcal{L}_4$, generically written as $\mathcal{A}^{\mathrm{EChL}^{(2+4)}_{\mathrm{Tree}}} = \mathcal{A}^{\mathrm{EChL}^{(2)}_{\mathrm{Tree}}} + \mathcal{A}^{\mathrm{EChL}^{(4)}_{\mathrm{Tree}}}$, whereas the one-loop correction, $\mathcal{O}(\hbar^1)$, is obtained by computing loops with just $\mathcal{L}_2$, generically written as $\mathcal{A}^{\mathrm{EChL}^{(2)}_{\mathrm{Loop}}}$. Remember that within the EChL framework, the a_i coefficients in $\mathcal{L}_4$ have a double role and will act as well as counterterms of the extra divergences generated by these loops which cannot be absorbed by just the renormalization of the parameters in $\mathcal{L}_2$.

On the other hand, we wish to compare the EChL predictions with the SM ones using the same procedure of 1PI functions. Thus, we will present in parallel the two predictions for the EChL and SM cases. To our knowledge, our SM computation is the first full bosonic one-loop computation of $WW \to HH$ scattering using the R_ξ gauges in the literature. This SM amplitude is defined as the sum of the LO contribution, which in this case is the tree-level contribution of $\mathcal{O}(\hbar^0)$, and the NLO contribution, which is that of $\mathcal{O}(\hbar^1)$:

$$\mathcal{A}^{\mathrm{SM_{Full}}} = \mathcal{A}^{\mathrm{SM_{Tree}}} + \mathcal{A}^{\mathrm{SM_{Loop}}}. \tag{3.5}$$

For the technical description of the one-loop radiative corrections, we then organize the one-loop full amplitude in terms of the 1PI Green's functions as follows:

$$\begin{aligned}\mathcal{A}^{\mathrm{EChL_{Full}}} &= \mathcal{A}^{\mathrm{LO}} + \mathcal{A}_{\text{1-leg}} + \mathcal{A}_{\text{2-legs}} + \mathcal{A}_{\text{3-legs}} \\ &\quad + \mathcal{A}_{\text{4-legs}} + \mathcal{A}_{\mathrm{res}}, \end{aligned} \tag{3.6}$$

where $\mathcal{A}^{\mathrm{LO}}$ is the result from the LO Lagrangian—i.e., $\mathcal{A}^{\mathrm{LO}} = \mathcal{A}^{(0)}$—and $\mathcal{A}_{n\text{-legs}}$ means the contributions to the amplitude from the n-legs 1PI functions. The LO contribution is that from $\mathcal{L}_2$ to tree level, and therefore it is $\mathcal{O}(\hbar^0)$. The $\mathcal{A}_{n\text{-legs}}$ terms contain the NLO contributions, including the contributions from the a_i coefficients and also the $\mathcal{O}(\hbar^1)$ contributions from the loop diagrams in the corresponding 1PI functions. Notice also that we have separated explicitly the extra contribution to the amplitude from the finite residues of the external particles $\mathcal{A}_{\mathrm{res}}$.

From now on, we fix the notation for the momenta assignments and Lorentz indexes for the process of interest as follows:

$$W^+_\mu(p_+)W^-_\nu(p_-) \to H(k_1)H(k_2), \tag{3.7}$$

where $p_{+,-}$ are the incoming momenta of the gauge bosons, with polarization vectors $\epsilon^\mu_+ \equiv \epsilon^\mu(p_+)$ and $\epsilon^\nu_- \equiv \epsilon^\nu(p_-)$, respectively, and $k_{1,2}$ are the outgoing momenta of the Higgs bosons (with $p_+ + p_- = k_1 + k_2$). Thus, the amplitude $\mathcal{A}$ can be written as

$$\mathcal{A} = A_{\mu\nu}\epsilon^\mu_+\epsilon^\nu_-, \tag{3.8}$$

where the tensor amplitude with explicit Lorentz indices is defined by $A_{\mu\nu}$. Figure 1 collects the full 1PI functions and full propagators, represented by black balls, that contribute to the one-loop amplitude $\mathcal{A}(WW \to HH)$. These full functions (denoted with a hat) correspond to (i) the full propagators, $\hat{\Delta}^{HH}$, $\hat{\Delta}^{\pi\pi}$, $\hat{\Delta}^{WW}$, $\hat{\Delta}^{W\pi}$, $\hat{\Delta}^{\pi W}$, $\hat{\Delta}^{AA}$, and $\hat{\Delta}^{ZZ}$; (ii) the full 1PI vertex functions with three legs, $\hat{\Gamma}_{HWW}$, $\hat{\Gamma}_{\pi WH}$, $\hat{\Gamma}_{HHH}$, $\hat{\Gamma}_{AWW}$, $\hat{\Gamma}_{ZWW}$, $\hat{\Gamma}_{AHH}$, and $\hat{\Gamma}_{ZHH}$; and (iii) the full 1PI vertex function with four legs, $\hat{\Gamma}_{WWHH}$. Notice that some of these full functions receive contributions of both orders, $\mathcal{O}(\hbar^0)$ and $\mathcal{O}(\hbar^1)$. However, there are some Green's functions that vanish at LO and only receive contributions from NLO, such as $\hat{\Delta}^{W\pi}$, $\hat{\Delta}^{\pi W}$, $\hat{\Gamma}_{AHH}$, and $\hat{\Gamma}_{ZHH}$. This is the reason why the diagrams in Fig. 1 involving these particular NLO Green's functions have only one black ball, since including two black balls in this case would produce NNLO

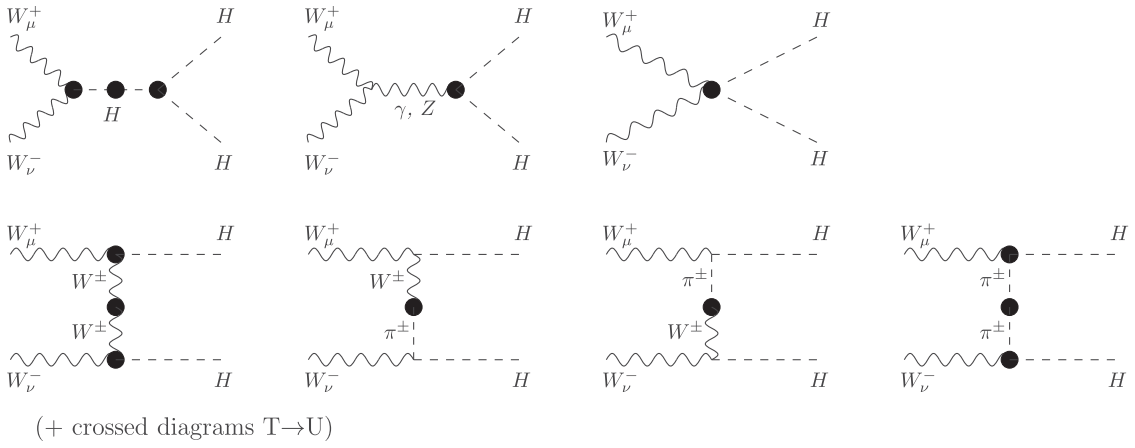

FIG. 1. Full 1PI functions (black balls) contributing to the full one-loop amplitude $\mathcal{A}(W^+W^- \to HH)$.

corrections that are not our aim here. For the other diagrams, not involving these particular 1PI functions, there can appear the product of several black balls, each one containing both LO and NLO contributions, and one has to perform this product accordingly to extract the final result for the amplitude containing all the terms of both orders, $\mathcal{O}(\hbar^0)$ and $\mathcal{O}(\hbar^1)$.

The tensor amplitude in Eq. (3.8) is obtained by adding the s, t, u, and contact (c) channel contributions as represented in Fig. 1. Notice that through this work we use both notations to the Mandelstam variables with small and capital letters equally. These contributions by channels can be written in terms of the full Green's functions as follows:

$$\begin{aligned}
iA_s^{\mu\nu} &= i\hat{\Gamma}^{\mu\nu}_{HWW} i\hat{\Delta}^{HH} i\hat{\Gamma}_{HHH} \\
&\quad + i\hat{\Gamma}^{\mu\nu\rho}_{WWA}(-i)\hat{\Delta}^{AA}_{\rho\sigma} i\hat{\Gamma}^{\sigma}_{AHH} + i\hat{\Gamma}^{\mu\nu\rho}_{WWZ}(-i)\hat{\Delta}^{ZZ}_{\rho\sigma} i\hat{\Gamma}^{\sigma}_{ZHH}, \\
iA_t^{\mu\nu} &= i\hat{\Gamma}^{\mu\rho}_{HWW}(-i)\hat{\Delta}^{WW}_{\rho\sigma} i\hat{\Gamma}^{\sigma\nu}_{HWW} + i\Gamma^{\mu\rho}_{HWW}\hat{\Delta}^{W\pi}_{\rho} i\Gamma^{\nu}_{\pi WH} \\
&\quad + i\Gamma^{\mu}_{\pi WH}\hat{\Delta}^{\pi W}_{\sigma} i\Gamma^{\sigma\nu}_{HWW} + i\hat{\Gamma}^{\mu}_{\pi WH} i\hat{\Delta}^{\pi\pi} i\hat{\Gamma}^{\nu}_{\pi WH}, \\
iA_u^{\mu\nu} &= i\hat{\Gamma}^{\mu\rho}_{HWW}(-i)\hat{\Delta}^{WW}_{\rho\sigma} i\hat{\Gamma}^{\sigma\nu}_{HWW} + i\Gamma^{\mu\rho}_{HWW}\hat{\Delta}^{W\pi}_{\rho} i\Gamma^{\nu}_{\pi WH} \\
&\quad + i\Gamma^{\mu}_{\pi WH}\hat{\Delta}^{\pi W}_{\sigma} i\Gamma^{\sigma\nu}_{HWW} + i\hat{\Gamma}^{\mu}_{\pi WH} i\hat{\Delta}^{\pi\pi} i\hat{\Gamma}^{\nu}_{\pi WH}, \\
iA_c^{\mu\nu} &= i\hat{\Gamma}^{\mu\nu}_{WWHH}.
\end{aligned} \tag{3.9}$$

At one-loop level, it is convenient to write the full propagators in terms of the self-energies. Following our procedure and conventions defined in Ref. [3], we get the following expressions for the full propagators in terms of the LO propagators and the full self-energies:

$$\begin{aligned}
i\hat{\Delta}^{HH}(q^2) &= i\Delta^{HH} + i\Delta^{HH}(-i)\hat{\Sigma}_{HH} i\Delta^{HH}, \\
i\hat{\Delta}^{\pi\pi}(q^2) &= i\Delta^{\pi\pi} + i\Delta^{\pi\pi}(-i)\hat{\Sigma}_{\pi\pi} i\Delta^{\pi\pi}, \\
-i\hat{\Delta}^{WW}_T(q^2) &= -i\Delta^{WW}_T - i\Delta^{WW}_T i\hat{\Sigma}^{T}_{WW}(-i)\Delta^{WW}_T, \\
-i\hat{\Delta}^{WW}_L(q^2) &= -i\Delta^{WW}_L - i\Delta^{WW}_L i\hat{\Sigma}^{L}_{WW}(-i)\Delta^{WW}_L, \\
\hat{\Delta}^{W\pi}(q^2) &= \Delta^{W\pi} - i\Delta^{WW}_L \hat{\Sigma}_{W\pi} i\Delta^{\pi\pi},
\end{aligned} \tag{3.10}$$

where all functions on the right-hand side are functions of q^2, and the LO propagators in the R_ξ gauges are summarized by

$$\begin{aligned}
&i\Delta^{HH} = \frac{i}{q^2 - m_{\rm H}^2}, \qquad -i\Delta^{WW}_T = \frac{-i}{q^2 - m_{\rm W}^2}, \\
&-i\Delta^{WW}_L = \frac{-i\xi}{q^2 - \xi m_{\rm W}^2}, \qquad i\Delta^{\pi\pi} = \frac{i}{q^2 - \xi m_{\rm W}^2}, \qquad \Delta^{W\pi} = 0. \\
&-i\Delta^{AA}_T = \frac{-i}{q^2}, \qquad -i\Delta^{AA}_L = \frac{-i\xi}{q^2}, \qquad -i\Delta^{ZZ}_T = \frac{-i}{q^2 - m_{\rm Z}^2}, \\
&-i\Delta^{ZZ}_L = \frac{-i\xi}{q^2 - \xi m_{\rm Z}^2}.
\end{aligned} \tag{3.11}$$

As commented previously, only Δ^{HH}, Δ^{WW}_T, Δ^{WW}_L, and $\Delta^{\pi\pi}$ are involved in the LO contribution to the amplitude in Eq. (3.1). On the other hand, the relevant vertex functions at LO are

$$\begin{aligned}
&i\Gamma^{\mu\nu}_{HWW} = iagm_{\rm W} g^{\mu\nu}, \qquad i\Gamma_{HHH} = -3i\kappa_3 m_{\rm H}^2/v, \\
&i\Gamma^{\mu}_{\pi WH} = agp^{\mu}_{\pi}, \qquad i\Gamma^{\mu\nu}_{WWHH} = ibg^2 g^{\mu\nu}/2.
\end{aligned} \tag{3.12}$$

Next, we present the computation of the LO amplitude using the R_ξ gauges. This can be easily done by plugging the corresponding LO functions of Eqs. (3.11) and (3.12) into Eq. (3.9)—namely, using Γ instead of $\hat{\Gamma}$, and Δ instead of $\hat{\Delta}$.

The result for the LO amplitude in the R_ξ gauge, corresponding to the tree-level diagrams in Fig. 2, is given by

$$A^{(0)} = A^{(0)}_s + A^{(0)}_t + A^{(0)}_u + A^{(0)}_c, \tag{3.13}$$

where the contributions by the s, t, u, and contact channels are given, respectively, by

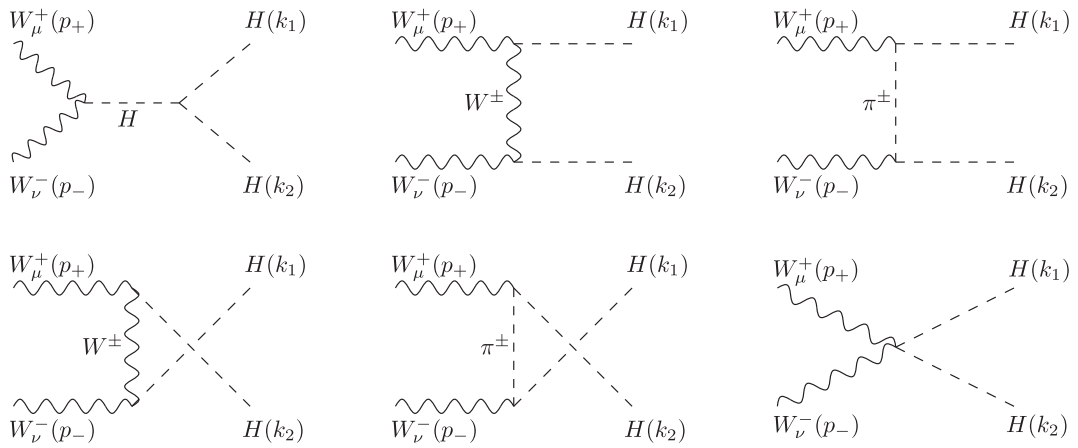

FIG. 2. Diagrams at LO contributing to $W^+W^- \to HH$ in the covariant R_ξ gauges.

$$
\begin{aligned}
A_s^{(0)} &= \frac{g^2}{2} 3a\kappa_3 \frac{m_{\rm H}^2}{S - m_{\rm H}^2} \epsilon_+ \cdot \epsilon_-, \\
A_t^{(0)} &= g^2 a^2 \frac{m_{\rm W}^2 \epsilon_+ \cdot \epsilon_- + \epsilon_+ \cdot k_1 \epsilon_- \cdot k_2}{T - m_{\rm W}^2}, \\
A_u^{(0)} &= g^2 a^2 \frac{m_{\rm W}^2 \epsilon_+ \cdot \epsilon_- + \epsilon_+ \cdot k_2 \epsilon_- \cdot k_1}{U - m_{\rm W}^2}, \\
A_c^{(0)} &= \frac{g^2}{2} b \epsilon_+ \cdot \epsilon_-.
\end{aligned} \tag{3.14}
$$

From this equation, notice that the corresponding result of the SM amplitude at LO is simply obtained from this same formula by setting $a = b = \kappa_3 = 1$. We have checked explicitly the gauge invariance of our LO result above—namely, that the dependence on ξ disappears in the final amplitude as expected. The cancellation of the ξ-dependent terms is achieved once the external gauge bosons are on shell—i.e., by contracting the tensorial amplitude with their corresponding polarization vectors in $\mathcal{A}^{(0)}$. Concretely, the cancellation of the ξ-dependent terms occurs separately in the two channels t and u, and it happens between the contribution of the longitudinal part of the W propagator and the GB propagator in Eq. (3.9).

Finally, we present the result for the complete amplitude to tree level—i.e.,

$$
\mathcal{A}^{\mathrm{EChL}^{(2+4)}_{\mathrm{Tree}}} = \mathcal{A}^{\mathrm{EChL}^{(2)}_{\mathrm{Tree}}} + \mathcal{A}^{\mathrm{EChL}^{(4)}_{\mathrm{Tree}}}, \tag{3.15}
$$

where $\mathcal{A}^{\mathrm{EChL}^{(2)}_{\mathrm{Tree}}} = A^{(0)}$ is given in Eqs. (3.13) and (3.14), and $\mathcal{A}^{\mathrm{EChL}^{(4)}_{\mathrm{Tree}}}$ is computed from $\mathcal{L}_4$ and contains the a_i coefficients. As we have explained in the previous section, this can be written in two ways, depending on whether one uses the EOMs to reduce the list of operators or not. We provide here the short version—i.e., using $\mathcal{L}_4^{+\mathrm{EOMs}}$ in Eq. (2.12):

$$
\begin{aligned}
\mathcal{A}^{\mathrm{EChL}^{(4)}_{\mathrm{Tree}}} = {} & \mathcal{A}^{\mathrm{EChL}^{(4)}_{\mathrm{Tree}}}\big|_s + \mathcal{A}^{\mathrm{EChL}^{(4)}_{\mathrm{Tree}}}\big|_t + \mathcal{A}^{\mathrm{EChL}^{(4)}_{\mathrm{Tree}}}\big|_u \\
& + \mathcal{A}^{\mathrm{EChL}^{(4)}_{\mathrm{Tree}}}\big|_c,
\end{aligned} \tag{3.16}
$$

where the contributions by channels are

$$
\begin{aligned}
\mathcal{A}^{\mathrm{EChL}^{(4)}_{\mathrm{Tree}}}\big|_s = {} & \frac{g^2}{2v^2} \frac{1}{S - m_{\rm H}^2} (3\kappa_3 a_{d2} m_{\rm H}^2 (S \epsilon_+ \cdot \epsilon_- - 2\epsilon_+ \cdot p_- \epsilon_- \cdot p_+) \\
& + 6\kappa_3 a_{HWW} m_{\rm H}^2 ((S - 2m_{\rm W}^2)\epsilon_+ \cdot \epsilon_- - 2\epsilon_+ \cdot p_- \epsilon_- \cdot p_+) \\
& - (3\kappa_3 \tilde{a}_{H\mathcal{V}\mathcal{V}} m_{\rm H}^4 + a(\tilde{a}_{Hdd} m_{\rm H}^2 + a_{ddW} m_{\rm W}^2 + a_{ddZ} m_{\rm Z}^2)(S + 2m_{\rm H}^2))\epsilon_+ \cdot \epsilon_-), \\
\mathcal{A}^{\mathrm{EChL}^{(4)}_{\mathrm{Tree}}}\big|_t = {} & \frac{g^2}{2v^2} \frac{a}{T - m_{\rm W}^2} (a_{d2}(4m_{\rm W}^2 m_{\rm H}^2 \epsilon_+ \cdot \epsilon_- + 2(T + 3m_{\rm W}^2 - m_{\rm H}^2)\epsilon_+ \cdot k_1 \epsilon_- \cdot k_2 \\
& - 4m_{\rm W}^2 (\epsilon_+ \cdot k_1 \epsilon_- \cdot p_+ + \epsilon_+ \cdot p_- \epsilon_- \cdot k_2)) \\
& - 8a_{HWW} m_{\rm W}^4 ((T + m_{\rm W}^2 - m_{\rm H}^2)\epsilon_+ \cdot \epsilon_- + \epsilon_+ \cdot k_1 \epsilon_- \cdot p_+ + \epsilon_+ \cdot p_- \epsilon_- \cdot k_2) \\
& - 4\tilde{a}_{H\mathcal{V}\mathcal{V}} m_{\rm H}^2 (m_{\rm W}^2 \epsilon_+ \cdot \epsilon_- + \epsilon_+ \cdot k_1 \epsilon_- \cdot k_2)),
\end{aligned}
$$

$$\mathcal{A}^{\mathrm{EChL}^{(4)}_{\mathrm{Tree}}}|_u = \mathcal{A}^{\mathrm{EChL}^{(4)}_{\mathrm{Tree}}}|_t \quad \text{with} \quad T \to U \quad \text{and} \quad k_1 \leftrightarrow k_2,$$

$$\begin{aligned}\mathcal{A}^{\mathrm{EChL}^{(4)}_{\mathrm{Tree}}}|_c = \frac{g^2}{2v^2}&(-2\tilde{a}_{dd\mathcal{V}\mathcal{V}1}(\epsilon_+ \cdot k_2 \epsilon_- \cdot k_1 + \epsilon_+ \cdot k_1 \epsilon_- \cdot k_2) \\ &+ (-2\tilde{a}_{dd\mathcal{V}\mathcal{V}2}(S - 2m_{\mathrm{H}}^2) + 4a_{HHWW}(S - 2m_{\mathrm{W}}^2) + a_{Hd2}S - \tilde{a}_{HH\mathcal{V}\mathcal{V}}m_{\mathrm{H}}^2)\epsilon_+ \cdot \epsilon_- \\ &- 2(a_{Hd2} + 4a_{HHWW})\epsilon_+ \cdot p_- \epsilon_- \cdot p_+). \end{aligned} \tag{3.17}$$

Notice that we have used the new coefficients defined in Eq. (2.13). Notice also that the above results are given in terms of the polarization vectors of the initial W gauge bosons. Therefore, our results above apply to all the possible polarized channels, $W_X W_Y \to HH$, with $XY = LL, TT, LT, TL$ by just inserting the proper polarization vectors ϵ_+ and ϵ_-.

We next comment shortly on the comparison of our analytical results in this section for the tree-level amplitude within the EChL with the previous literature. First of all, the LO amplitude in Eqs. (3.13) and (3.14) is in full agreement with Ref. [12]. Secondly, regarding $\mathcal{A}^{\mathrm{EChL}^{(4)}_{\mathrm{Tree}}}$, we have compared our results with those in Ref. [5]. We have checked the full agreement in the contributions from the coefficients, $\tilde{a}_{dd\mathcal{V}\mathcal{V}1}$ $(= \eta)$, $\tilde{a}_{dd\mathcal{V}\mathcal{V}2}$ $(= \delta)$, a_{d2} $(= b_1\chi)$, and a_{Hd2} $(= 2b_2\chi)$ with their results. The other coefficients in our result of Eq. (3.17) were not considered in Ref. [5]. On the other hand, the results of Ref. [4] in terms of δ and η were provided using the equivalence theorem, so they can only be compared for the longitudinal modes and in the high-energy regime $\sqrt{s} \gg m_{\mathrm{W}}, m_{\mathrm{H}}$. By an exploration of our amplitudes for the case of the longitudinal modes in that high-energy regime, we have also checked the agreement of the η and δ contributions with that reference. The other parameters were not studied either in that reference.

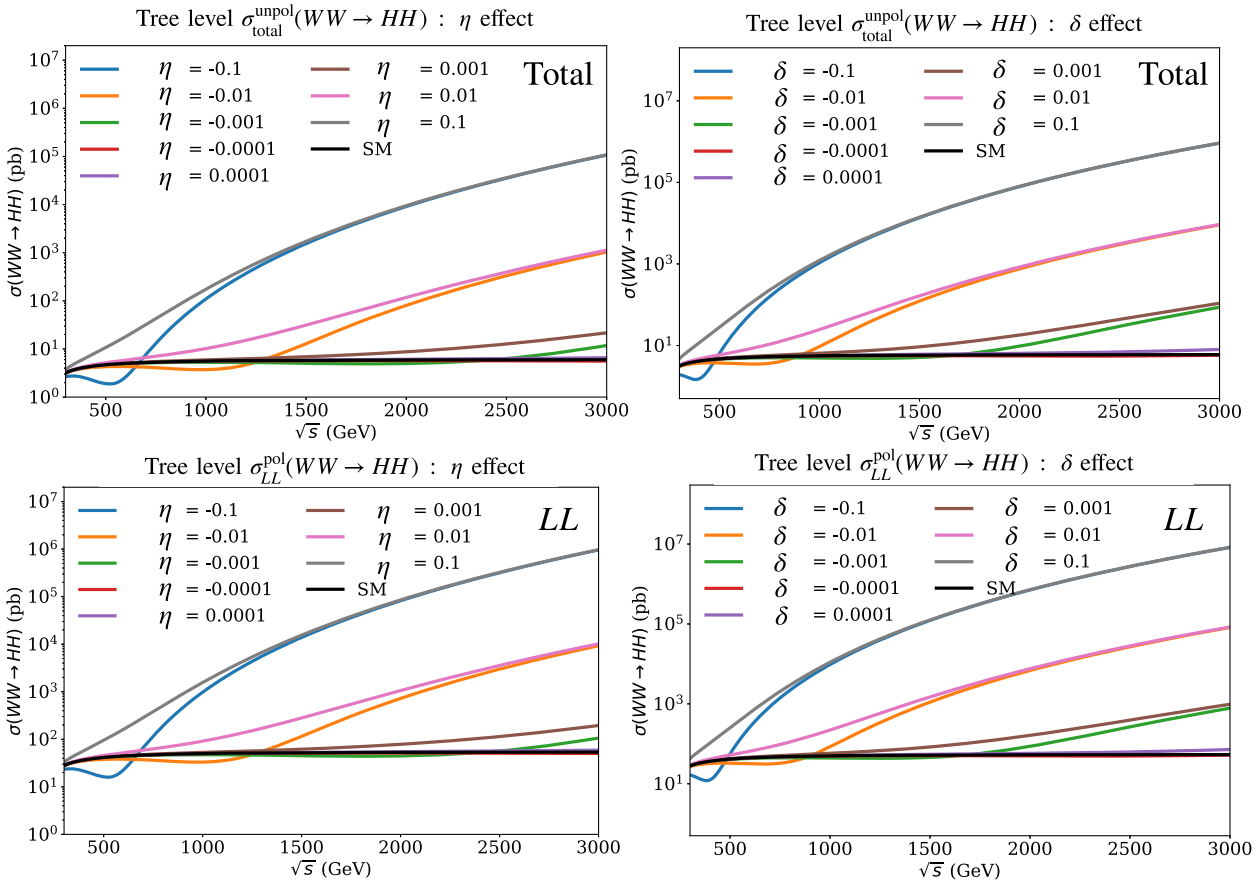

FIG. 3. Tree-level cross section predictions for $W^+W^- \to HH$ within the EChL, setting $a = b = \kappa_3 = \kappa_4 = 1$. All EChL coefficients in the NLO Lagrangian are set to zero except for η and δ. Plots in the left column are for nonvanishing η, and plots in the right column are for nonvanishing δ. The predictions for the total unpolarized case are displayed in the plots of the first row, and those for the polarized LL case in the second row. The SM predictions are displayed in all the plots for comparison.

Finally, it is important to keep in mind the existent hierarchy among the various polarization channels and among the relevance of the various coefficients for each polarization channel. First, it is well known the dominance in the total cross section for this $WW \to HH$ process of the longitudinal polarized modes over the transverse modes. Namely, $\sigma(WW \to HH)$ is fully dominated by $\sigma(W_L W_L \to HH)$. The other polarization channels with initial $W_T W_T$ or $W_L W_T$ are highly subdominant at the center-of-mass energies in the TeV domain. Therefore, by studying the longitudinal polarized case, one can approximate quite well the total cross section. This dominance of $\sigma(W_L W_L \to HH)$ over the other polarized channels also happens in the EChL case, in the tree-level estimates of the cross section, at both orders—the LO and the NLO ones. A recent phenomenological study of the corresponding BSM effects in Ref. [11] for all the polarized channels, and considering all the EChL coefficients in Eq. (3.17), has shown that the most relevant coefficients of the EChL, for the LL modes and at the tree-level NLO, are indeed η and δ. Here, by "the most relevant coefficients" we mean those EChL coefficients in $\mathcal{L}_4$ that lead to the largest cross sections in this $WW \to HH$ scattering process at the TeV energy domain. For definiteness here, and to summarize this LL dominance in the tree-level NLO prediction from the EChL, we show in Fig. 3 our predictions, as a function of the center-of-mass energy $\sqrt{s}$, of the cross sections (i) for the total unpolarized case (the two plots on the first row), and (ii) for the LL polarized case (the two plots on the second row). We display in this figure the BSM departures with respect to the SM predictions from the separate effects of the two most relevant coefficients, assuming different numerical values for those coefficients $\pm(0.1, 0.01, 0.001, 0.0001)$. (i) The effect from η is displayed in the plots in the first column, and (ii) the effect from δ is displayed in the plots in the second column. We can clearly see in these plots that the cross section for the LL case fully dominates the total (unpolarized) cross section for all the studied cases. Indeed, the two lines for LL and for "total" practically coincide in the studied TeV domain (up to the obvious reducing $1/9$ factor in the unpolarized result due to the average over the possible initial helicities). The other evident conclusion from this figure is that large values of the cross sections and large departures from the SM predictions can be reached at TeV energies for the cases with the larger input coefficients η and δ. For a more devoted study of the phenomenological consequences of these tree-level predictions within the EChL at NLO, we address the reader to Ref. [11]. In particular, the relevance of these predictions for the di-Higgs production at future e^+e^- colliders via WW fusion has also been explored in that reference. In the following part of the present work, we do not go further in these phenomenological issues and focus instead in our main purpose here: the computation of the EW radiative corrections for the $WW \to HH$ scattering process.

IV. RENORMALIZATION PROCEDURE

A. Generalities

In this section, we present our renormalization program to compute the renormalized 1PI functions within the EChL in covariant R_ξ gauges using a diagrammatic approach. These renormalized 1PI functions, denoted here generically by $\hat{\Gamma}$, receive contributions from the tree-level Lagrangian $\mathcal{L}_2 + \mathcal{L}_4$, Γ^{Tree}; from the one-loop diagrams using the interaction vertices of $\mathcal{L}_2$ only, Γ^{Loop}; and from all the counterterms of $\mathcal{L}_2 + \mathcal{L}_4$, Γ^{CT}:

$$\hat{\Gamma}_{n\text{-legs}} = \Gamma^{\text{Tree}}_{n\text{-legs}} + \Gamma^{\text{Loop}}_{n\text{-legs}} + \Gamma^{\text{CT}}_{n\text{-legs}}. \tag{4.1}$$

Notice again the double role of $\mathcal{L}_4$ in the chiral Lagrangian approach: on the one hand, it contributes to a tree-level scattering amplitude, and on the other hand it also acts as a source of new counterterms in order to remove the extra divergences emerging from the loops computed with $\mathcal{L}_2$, which are not removable by a simple redefinition of the parameters in this part of the Lagrangian.

Our analytical computation here is performed with the various software associated with Wolfram *Mathematica* [13] and starts by implementing our model in FeynRules [14], generating and drawing the Feynman diagrams with FeynArts [15] and performing the main calculations with FormCalc and LoopTools [16]. Some extra checks of the involved one-loop divergences were made using FeynCalc [17] and Package-X [18]. The SM results were obtained by following the same steps.

The renormalization program followed in this work is similar to the one we already presented in Ref. [3] in the EChL context for vector boson scattering (VBS) processes like $WZ \to WZ$, etc. Next, we briefly summarize the main aspects of the regularization and multiplicative renormalization prescriptions, as well as the renormalization conditions; and then we present the new one-loop diagrams, the new divergences, and the solutions for all the counterterms relevant for $WW \to HH$ scattering.

B. Regularization and renormalization prescriptions

As usual, our regularization procedure of the loop contributions is performed with dimensional regularization [19,20] in $D = 4 - \epsilon$ dimensions. This method preserves all the relevant symmetries in the bosonic sector of the theory, including chiral invariance (Dirac γ_5 is not involved in this work, since we do not consider the fermionic contributions). Consequently, the scale of dimensional regularization is set to μ, and all the one-loop divergences are expressed in terms of

$$\Delta_\epsilon = \frac{2}{\epsilon} - \gamma_E + \log(4\pi). \tag{4.2}$$

Concerning the renormalization procedure, we generate the counterterms of all the parameters and fields appearing in the tree-level Lagrangian, $\mathcal{L}_2 + \mathcal{L}_4$, by the usual multiplicative renormalization prescription that relates the bare quantities (here denoted by a specific sub- or superscript with a label 0) and the renormalized ones (here with no specific sub- or superscript labels). We have the following relations:

$$\begin{aligned}
&H_0 = \sqrt{Z_H}H, \qquad B_{0\mu} = \sqrt{Z_B}B_\mu, \qquad W^{1,2,3}_{0\mu} = \sqrt{Z_W}W^{1,2,3}_\mu, \qquad \pi^{1,2,3}_0 = \sqrt{Z_\pi}\pi^{1,2,3},\\
&v_0 = \sqrt{Z_\pi}(v+\delta v), \qquad \lambda_0 = Z_H^{-2}(\lambda+\delta\lambda),\\
&g'_0 = Z_B^{-1/2}(g'+\delta g'), \qquad g_0 = Z_W^{-1/2}(g+\delta g), \qquad \xi^0_{1,2} = \xi(1+\delta\xi_{1,2}),\\
&a^0 = a+\delta a, \qquad b^0 = b+\delta b, \qquad \kappa^0_{3,4} = \kappa_{3,4}+\delta\kappa_{3,4}, \qquad a^0_i = a_i+\delta a_i,
\end{aligned} \tag{4.3}$$

where $Z_i = 1 + \delta Z_i$ are the usual renormalization multiplicative constants, and we use the generic notation δp (δa_i) for the counterterm of each involved EW parameter p (effective coefficient a_i).

With these definitions, our final results for both the renormalized 1PI functions and the $WW \to HH$ scattering amplitude are expressed in terms of the renormalized quantities: $m_{\rm W}$, $m_{\rm Z}$, $m_{\rm H}$, g, g', v, a, b, κ_3, λ, and the a_i's. Notice that κ_4 and the ghost counterterms do not enter into the present computation, and we omit them for brevity. On the other hand, the renormalization of the covariant gauge-fixing parameters have set a common renormalized ξ parameter for all the involved EW gauge bosons. For more details on the technicalities of our renormalization method, see Ref. [3].

Next, we summarize the renormalization conditions. As in Ref. [3], we adopt here a hybrid prescription in which we choose the on-shell (OS) scheme for the EW parameters in the lowest-order Lagrangian $\mathcal{L}_2$ and the $\overline{\rm MS}$ scheme for all the EChL coefficients. The list of conditions are as follows:

(1) Vanishing (Higgs) tadpole:

$$\hat{T} = 0. \tag{4.4}$$

(2) The pole of the renormalized propagator of the Higgs boson lies at $m^2_{\rm H}$, and the corresponding residue is equal to 1:

$$\mathrm{Re}[\hat{\Sigma}_{HH}(m^2_{\rm H})] = 0, \quad \mathrm{Re}\left[\frac{d\hat{\Sigma}_{HH}}{dq^2}(m^2_{\rm H})\right] = 0. \tag{4.5}$$

(3) Properties of the photon: the residue equals 1, there are no $A-Z$ mixing propagators, and the electric charge is defined like in QED, since there is a remnant $U(1)_{\rm em}$ electromagnetic gauge symmetry:

$$\mathrm{Re}\left[\frac{d\hat{\Sigma}^T_{AA}}{dq^2}(0)\right] = 0, \quad \hat{\Sigma}^T_{ZA}(0) = 0, \quad \hat{\Gamma}^\mu_{\gamma ee}|_{\rm OS} = ie\gamma^\mu. \tag{4.6}$$

(4) The poles of the transverse renormalized propagators of the W and Z bosons lie at $q^2 = m^2_{\rm W}$ and $q^2 = m^2_{\rm Z}$, respectively:

$$\mathrm{Re}[\hat{\Sigma}^T_{WW}(m^2_{\rm W})] = 0, \qquad \mathrm{Re}[\hat{\Sigma}^T_{ZZ}(m^2_{\rm Z})] = 0. \tag{4.7}$$

(5) The poles of the renormalized propagators in the unphysical charged sector $\{W^\pm, \pi^\pm\}$ lie at $q^2 = \xi m^2_{\rm W}$. Therefore,

$$\mathrm{Re}[\hat{\Sigma}^L_{WW}(\xi m^2_{\rm W})] = 0, \quad \mathrm{Re}[\hat{\Sigma}_{\pi\pi}(\xi m^2_{\rm W})] = 0. \tag{4.8}$$

(6) $\overline{\rm MS}$ scheme for all the involved EChL coefficients: In particular, this applies for a, b, κ_3, κ_4 in Eq. (2.4) and the a_i's in Eq. (2.10).

The above renormalization conditions on all the EChL parameters determine both the divergent and finite parts involved in all the 1PI functions, and therefore also in the one-loop scattering amplitudes. Notice that the residues for the Higgs and photon fields are set to 1 in the previous conditions, but the resulting residues $\mathcal{Z}_{W(Z)}$ of the gauge bosons $W(Z)$ are different from 1. Since each external W provides a factor $\mathcal{Z}_W^{1/2}$ to the observable S matrix, the corresponding contribution from the residues [$\mathcal{A}_{\rm res}$ in Eq. (3.6)] of the two external W's in $WW \to HH$ scattering is given by

$$\mathcal{A}_{\rm res} = \mathrm{Re}\left[\frac{d\hat{\Sigma}^T_{WW}}{dq^2}(m^2_{\rm W})\right]\mathcal{A}^{(0)}. \tag{4.9}$$

In addition, the Higgs tadpole enters into many parts of the different diagrams contributing to the amplitude. However, with the renormalization condition of Eq. (4.4), the $\mathcal{A}_{\text{1-leg}}$ in Eq. (3.6) vanishes.

C. Summary of contributions to the renormalized 1PI functions

We emphasize again that our renormalization program in the R_ξ gauges makes finite all the relevant 1PI Green's

functions for arbitrary momentum of the external legs (hence, generically, off shell); and no transversality condition for the EW gauge bosons, $p_i \cdot \epsilon(p_i) = 0$, is applied for those 1PI results. This means that our renormalization program is more demanding than the usual renormalization program, which gets just finite results for the scattering amplitudes with on-shell external legs. Notice also that in this latter case, the transversality conditions for the external gauge bosons are usually used as well.

In the following part of this section, we collect the various contributions to the renormalized 1PI functions, already mentioned in Sec. III, that enter into $WW \to HH$ scattering and that were not involved in our previous computation [3], which was addressed to the $WZ \to WZ$ case. In particular, we exhibit now the results for the Green's functions involving Higgs bosons in the external legs, corresponding to the vertices HHH, HWW, πWH, AHH, ZHH, and $WWHH$. And, for completeness, we also include in Appendix A a short summary of the other renormalized 1PI functions derived in Ref. [3] that also enter here for the $WW \to HH$ scattering. For definiteness, all the explicit analytical results presented in the present paper (and in the appendices) are provided in the Feynman–'t Hooft gauge with $\xi = 1$.

The results of the three-legs functions corresponding to $H(p_1)H(p_2)H(p_3)$, $H(q)W^\mu(k_1)W^\nu(k_2)$, $\pi(q)W^\mu(p_W)H(p_H)$, and $V^\rho(q)H(p_1)H(p_2)$ (with $V = A, Z$) are given by the sum of the LO part (if any), loop contributions, EFT coefficients' contributions, and CT contributions, as follows:

$$
\begin{aligned}
i\hat{\Gamma}_{HHH} &= -3i\kappa_3 \frac{m_{\rm H}^2}{v} + i\Gamma^{\rm Loop}_{HHH} - 3i\kappa_3 \frac{m_{\rm H}^2}{v}\left(\frac{\delta\kappa_3}{\kappa_3} + \frac{\delta m_{\rm H}^2}{m_{\rm H}^2} - \frac{\delta Z_\pi}{2} - \frac{\delta v}{v} + \frac{3\delta Z_H}{2}\right) \\
&\quad + \frac{i}{v^3}(a_{dd\Box}(p_1^4 + p_2^4 + p_3^4) + 2(a_{H\Box\Box} - a_{dd\Box})(p_1^2p_2^2 + p_2^2p_3^2 + p_3^2p_1^2) \\
&\quad + (a_{Hdd}m_{\rm H}^2 + a_{ddW}m_{\rm W}^2 + a_{ddZ}m_{\rm Z}^2)(p_1^2 + p_2^2 + p_3^2)), \\
i\hat{\Gamma}^{\mu\nu}_{HW^-W^+} &= ia\frac{g^2v}{2}g^{\mu\nu} + i\Gamma^{\rm Loop}_{HWW} + i\frac{ag^2v}{2}\left(\frac{\delta a}{a} + \frac{2\delta g}{g} + \frac{\delta v}{v} + \frac{\delta Z_H}{2} + \frac{\delta Z_\pi}{2}\right)g^{\mu\nu} \\
&\quad - i\frac{g^2}{2v}((-(2a_{HWW} + a_{d2} + 2a_{\Box\mathcal{V}\mathcal{V}})q^2 + 2a_{HWW}(k_1^2 + k_2^2) + a_{H\mathcal{V}\mathcal{V}}m_{\rm H}^2)g^{\mu\nu} \\
&\quad + (a_{d2} + a_{d3})(k_1^\mu k_1^\nu + k_2^\mu k_2^\nu) + 2(a_{d3} - a_{H11})k_1^\mu k_2^\nu + 2(2a_{HWW} + a_{d2})k_2^\mu k_1^\nu), \\
i\hat{\Gamma}^{\mu}_{\pi^+W^-H} &= -iag(p_W + p_H)^\mu + i\Gamma^{\rm Loop}_{\pi WH} - iag\left(\frac{\delta a}{a} + \frac{\delta g}{g} + \delta Z_H/2 + \delta Z_\pi/2\right)(p_W + p_H)^\mu \\
&\quad + i\frac{g}{2v^2}(-2(p_H^\mu + p_W^\mu)(2a_{\Box\mathcal{V}\mathcal{V}}p_H^2 + a_{d2}p_W^2 - a_{d3}q^2 - a_{H\mathcal{V}\mathcal{V}}m_{\rm H}^2) \\
&\quad + p_W^\mu q^2(a_{d2} - 3a_{d3} + 4a_{H11}) + p_W^\mu(a_{d2} + a_{d3})(p_W^2 - p_H^2)), \\
i\hat{\Gamma}^{\rho}_{AHH} &= i\Gamma^{\rm Loop}_{AHH}, \\
i\hat{\Gamma}^{\rho}_{ZHH} &= i\Gamma^{\rm Loop}_{ZHH}.
\end{aligned}
\tag{4.10}
$$

Similarly, the result of the four-legs function corresponding to $W^\mu(p_1)W^\nu(p_2)H(p_3)H(p_4)$ is given by the sum of the LO part, the loop contributions, the EFT coefficients contributions, and the CT contributions as follows:

$$
\begin{aligned}
i\hat{\Gamma}^{\mu\nu}_{W^+W^-HH} &= i\frac{bg^2}{2}g^{\mu\nu} + i\Gamma^{\rm Loop}_{WWHH} + i\frac{bg^2}{2}\left(\frac{\delta b}{b} + \frac{2\delta g}{g} + \delta Z_H\right)g^{\mu\nu} \\
&\quad - \frac{ig^2}{2v^2}(g^{\mu\nu}(-(p_3^2 + p_4^2)(-2a_{dd\mathcal{V}\mathcal{V}2} + 4a_{HHWW} + 2a_{H\Box\mathcal{V}\mathcal{V}}) + (p_1 + p_2)^2(-2a_{dd\mathcal{V}\mathcal{V}2} - a_{Hd2}) \\
&\quad + 4((p_1 + p_3)^2 + (p_1 + p_4)^2)a_{HHWW} + a_{HH\mathcal{V}\mathcal{V}}m_{\rm H}^2) \\
&\quad + 4(a_{HH11} - 2a_{HHWW})p_2^\mu p_2^\nu - (a_{Hd2} - a_{Hd3} + 8a_{HHWW})p_2^\mu(p_3^\nu + p_4^\nu) \\
&\quad + (a_{Hd2} - a_{Hd3} + 4a_{HHWW})(p_3^\mu + p_4^\mu)p_2^\nu + (a_{Hd2} + a_{Hd3})(p_3^\mu p_3^\nu + p_4^\mu p_4^\nu) \\
&\quad + (-2a_{dd\mathcal{V}\mathcal{V}1} + a_{Hd2} + a_{Hd3})(p_3^\mu p_4^\nu + p_4^\mu p_3^\nu)).
\end{aligned}
\tag{4.11}
$$

In all the previous expressions above, in Eqs. (4.10) and (4.11), the explicit a_i coefficients entering are the bare a_i^0 coefficients, but for shortness we have dropped the super-index 0. Therefore, the a_i's included in these equations must be all understood rather as $(a_i + \delta a_i)$, with these a_i's being the renormalized coefficients in the $\overline{\text{MS}}$, and δa_i being the corresponding divergent CT needed to cancel the new divergences from the loops of the 1PI functions. As we have said, the computation of the loop contributions to all these 1PI functions is performed with the help of FormCalc and LoopTools. For illustrative purposes, we show in Figs. 6 and 7 all the generic one-loop diagrams entering into the computation of the previous Γ^{loop} functions. Notice that since we are working with covariant R_ξ gauges, we have considered all the possible particles propagating in the loops—namely, GBs, Higgs, EW gauge bosons, and ghosts.

Next, we provide our results for the divergent (singular) parts of these loop contributions for the relevant 1PI functions in Eqs. (4.10) and (4.11). All these divergent contributions will set the values of the $\mathcal{O}(\Delta_\epsilon)$ counterterms, both for the EW parameters and the a_i coefficients, that are relevant for our computation. We get the following results:

$$
\begin{aligned}
i\Gamma^{\text{Loop}}_{HHH}|_{\text{div}} &= i\frac{\Delta_\epsilon}{16\pi^2}\frac{3}{2v^3}(9\kappa_3\kappa_4 m_{\text{H}}^4 + 12ab(2m_{\text{W}}^4 + m_{\text{Z}}^4) - 2a^3(p_1^2p_2^2 + p_2^2p_3^2 + p_3^2p_1^2)\\
&\quad - a(a^2-b)(p_1^4 + p_2^4 + p_3^4 - 2(2m_{\text{W}}^2 + m_{\text{Z}}^2)(p_1^2 + p_2^2 + p_3^2))),\\
i\Gamma^{\text{Loop}}_{HWW}|_{\text{div}} &= i\frac{\Delta_\epsilon}{16\pi^2}\frac{g^2}{12v}((3a(2+a^2)q^2 + a(a^2-b)(k_1^2 + k_2^2)\\
&\quad - 3(a^2-b)(2a-3\kappa_3)m_{\text{H}}^2 - 18abm_{\text{W}}^2 + 78am_{\text{W}}^2 - 18am_{\text{Z}}^2)g^{\mu\nu}\\
&\quad + 2a(a^2+2b)(k_1^\mu k_1^\nu + k_2^\mu k_2^\nu) + 12a^3k_1^\mu k_2^\nu),\\
i\Gamma^{\text{Loop}}_{\pi WH}|_{\text{div}} &= i\frac{\Delta_\epsilon}{16\pi^2}\frac{g}{6v^2}((p_H^\mu + p_W^\mu)(-9(a^2-b)\kappa_3 m_{\text{H}}^2 - a^3(3p_H^2 + p_W^2 - 6m_{\text{H}}^2 + 3q^2)\\
&\quad + a(-6p_H^2 - 34m_{\text{W}}^2 + 14m_{\text{Z}}^2 + b(p_W^2 - 6m_{\text{H}}^2 + 18m_{\text{W}}^2 - 3q^2)))\\
&\quad + p_W^\mu a((2 + a^2 + 2b)p_H^2 - a^2(p_W^2 - 11q^2) + 2(m_{\text{W}}^2 + m_{\text{Z}}^2 - b(p_W^2 + q^2)))),\\
i\Gamma^{\text{Loop}}_{AHH}|_{\text{div}} &= i\Gamma^{\text{Loop}}_{ZHH}|_{\text{div}} = 0,\\
i\Gamma^{\text{Loop}}_{WWHH}|_{\text{div}} &= -i\frac{\Delta_\epsilon}{16\pi^2}\frac{g^2}{12v^2}(g^{\mu\nu}(3(-8a^4 + 12a^3\kappa_3 - 12ab\kappa_3 + a^2(10b - 3\kappa_4) - 2b^2 + 3b\kappa_4)m_{\text{H}}^2\\
&\quad + 3b((6b-26)m_{\text{W}}^2 + 6m_{\text{Z}}^2)(p_3^2 + p_4^2)a^2(6 + 6a^2 - 3b)\\
&\quad + 6(p_1+p_2)^2(1+a^2)(a^2-b) + ((p_1+p_3)^2 + (p_1+p_4)^2)(4a^4 - 5a^2b + b^2))\\
&\quad - 8(4a^4 - 5a^2b + b^2)p_2^\mu p_2^\nu + 2(4a^4 + a^2b - 2b^2)p_2^\mu(p_3^\nu + p_4^\nu)\\
&\quad - 2(20a^4 - 19a^2b + 2b^2)(p_3^\mu + p_4^\mu)p_2^\nu + 2(4a^4 + a^2b - 2b^2)(p_3^\mu p_3^\nu + p_4^\mu p_4^\nu)\\
&\quad + 6a^2(2a^2 + b)(p_3^\mu p_4^\nu + p_4^\mu p_3^\nu)).
\end{aligned}
\tag{4.12}
$$

Finally, we present the corresponding results in the SM for the Green's functions that are involved in the $WW \to HH$ computation and were not given in Ref. [3]. We use the "bar" notation for all the 1PI functions in the SM, not to be confused with the previous functions of the HEFT. Notice that, contrary to the HEFT, in the SM case, the multiplicative renormalization constant for the Higgs and GBs fields are the same (Z_ϕ), since they form a doublet. We get the following SM results:

$$
\begin{aligned}
i\hat{\bar{\Gamma}}_{HHH} &= -3i\frac{m_{\text{H}}^2}{v} + i\bar{\Gamma}^{\text{Loop}}_{HHH} - 3i\frac{m_{\text{H}}^2}{v}\left(\frac{\delta m_{\text{H}}^2}{m_{\text{H}}^2} + \delta Z_\phi - \frac{\delta v}{v}\right),\\
i\bar{\Gamma}^{\text{Loop}}_{HHH}|_{\text{div}} &= i\frac{\Delta_\epsilon}{16\pi^2}\frac{3}{v^3}(6m_{\text{H}}^4 + 6(2m_{\text{W}}^4 + m_{\text{Z}}^4) - m_{\text{H}}^2(2m_{\text{W}}^2 + m_{\text{Z}}^2)),\\
i\hat{\bar{\Gamma}}^{\mu\nu}_{HW^+W^-} &= i\frac{g^2v}{2}g^{\mu\nu} + i\bar{\Gamma}^{\text{Loop}}_{HWW} + i\frac{g^2v}{2}\left(\frac{2\delta g}{g} + \frac{\delta v}{v} + \delta Z_\phi\right)g^{\mu\nu},\\
i\bar{\Gamma}^{\text{Loop}}_{HWW}|_{\text{div}} &= i\frac{\Delta_\epsilon}{16\pi^2}\frac{g^2}{2v}(10m_{\text{W}}^2 - 3m_{\text{Z}}^2)g^{\mu\nu},
\end{aligned}
$$

$$
\begin{aligned}
i\hat{\bar{\Gamma}}^{\mu}_{\pi WH} &= -i\frac{g}{2}(p_W+2p_H)^{\mu} + i\bar{\Gamma}^{\mathrm{Loop}}_{\pi WH} - i\frac{g}{2}\left(\frac{\delta g}{g}+\delta Z_{\phi}\right)(p_W+2p_H)^{\mu},\\
i\bar{\Gamma}^{\mathrm{Loop}}_{\pi WH}|_{\mathrm{div}} &= -i\frac{\Delta_\epsilon}{16\pi^2}\frac{g}{v^2}(2m_{\mathrm{W}}^2-m_{\mathrm{Z}}^2)(p_W+2p_H)^{\mu},\\
i\hat{\bar{\Gamma}}^{\mu\nu}_{WWHH} &= i\frac{g^2}{2}g^{\mu\nu} + i\bar{\Gamma}^{\mathrm{Loop}}_{WWHH} + i\frac{g^2}{2}\left(\frac{2\delta g}{g}+\delta Z_{\phi}\right)g^{\mu\nu},\\
i\bar{\Gamma}^{\mathrm{Loop}}_{WWHH}|_{\mathrm{div}} &= i\frac{\Delta_\epsilon}{16\pi^2}\frac{g^2}{v^2}(6m_{\mathrm{W}}^2-m_{\mathrm{Z}}^2)g^{\mu\nu},\\
i\hat{\bar{\Gamma}}^{\rho}_{AHH} &= i\bar{\Gamma}^{\mathrm{Loop}}_{AHH},\\
i\bar{\Gamma}^{\mathrm{Loop}}_{AHH}|_{\mathrm{div}} &= 0,\\
i\hat{\bar{\Gamma}}^{\rho}_{ZHH} &= i\bar{\Gamma}^{\mathrm{Loop}}_{ZHH},\\
i\bar{\Gamma}^{\mathrm{Loop}}_{ZHH}|_{\mathrm{div}} &= 0.
\end{aligned}
\tag{4.13}
$$

D. Renormalization of the EFT parameters

In this section, we present the results for the renormalization of the EFT parameters. These include the EW parameters entering in $\mathcal{L}_2$, like g, g', etc., and the EChL coefficients—namely, a, b, κ_3 entering in $\mathcal{L}_2$, and the a_i coefficients entering in $\mathcal{L}_4$.

First, we determine the divergent parts (called in short δ_ϵ) of all the counterterms, requiring that all the renormalized 1PI functions at arbitrary values of the external leg momenta (generically off-shell) results be finite. This procedure leads to a system of equations, which must be solved sequentially, by demanding the cancellation of the $\mathcal{O}(\Delta_\epsilon)$ contributions for the involved Lorentz structure and momentum dependence of each Green's functions. The CTs corresponding to the $\mathcal{L}_2$ parameters in Eq. (2.4), except for b, κ_3, and λ, and some of the a_i coefficients in Eq. (2.10), were already derived in our previous work [3]. With respect to this reference, we add now the Green's functions with Higgs bosons corresponding to the vertices HHH, HWW, πWH, and $WWHH$ (notice that the corresponding ones for AHH and ZHH are finite and do not have new EChL coefficients). In particular, we derive $\delta_\epsilon\lambda$ from the tadpole's counterterm; $\hat{\Gamma}_{HHH}$ sets $\delta_\epsilon\kappa_3$, $\delta_\epsilon a_{dd\Box}$, $\delta_\epsilon a_{H\Box\Box}$, and $\delta_\epsilon a_{Hdd}$; $\hat{\Gamma}_{HWW}$ sets $\delta_\epsilon a_{HWW}$, $\delta_\epsilon a_{d2}$, $\delta_\epsilon a_{\Box\mathcal{V}\mathcal{V}}$, $\delta_\epsilon a_{H\mathcal{V}\mathcal{V}}$, $\delta_\epsilon a_{d3}$, and $\delta_\epsilon a_{H11}$; $\hat{\Gamma}_{WWHH}$ sets $\delta_\epsilon b$, $\delta_\epsilon a_{dd\mathcal{V}\mathcal{V}1}$, $\delta_\epsilon a_{dd\mathcal{V}\mathcal{V}2}$, $\delta_\epsilon a_{HHWW}$, $\delta_\epsilon a_{HH11}$, $\delta_\epsilon a_{H\Box\mathcal{V}\mathcal{V}}$, $\delta_\epsilon a_{Hd2}$, $\delta_\epsilon a_{Hd3}$, and $\delta_\epsilon a_{HH\mathcal{V}\mathcal{V}}$; and with the singular parts of all the CTs, we check that $\hat{\Gamma}_{\pi WH}$ gives a finite contribution to the scattering amplitude.

Second, these divergent parts of the CTs can also be determined by using the renormalization conditions of Eqs. (4.4)–(4.8). They allow us to write the counterterms as functions of the undressed 1PI functions. Then we have used this second procedure as a check of our results that we obtain solving the system described in the previous paragraph. Also, with this second procedure, we can determine the finite contributions to the counterterms (if any), and we use them in the final numerical computation of the one-loop cross section in the next section. Therefore, we postpone the estimates of the finite contributions to the next section and focus here on the derivation of the singular parts of the EChL counterterms. For completeness, we also provide the divergent counterterms for the EW parameters derived in our previous work together with $\delta_\epsilon\lambda$ (that enters now in the s channel) in Eq. (A5). The corresponding SM results, obtained from the one-leg and two-leg Green's functions, were presented and compared with the EChL in Ref. [3], and we do not repeat them here.

Our results for the divergent parts of the full set of EChL coefficients are then summarized as follows:

$$
\begin{aligned}
\delta_\epsilon a &= \frac{\Delta_\epsilon}{16\pi^2}\frac{3}{2v^2}((a^2-b)(a-\kappa_3)m_{\mathrm{H}}^2 + a((1-3a^2+2b)m_{\mathrm{W}}^2+(1-a^2)m_{\mathrm{Z}}^2)),\\
\boldsymbol{\delta_\epsilon b} &= -\frac{\Delta_\epsilon}{16\pi^2}\frac{1}{2v^2}((a^2-b)(8a^2-2b-12a\kappa_3+3\kappa_4)m_{\mathrm{H}}^2\\
&\quad + 6a^2b(2m_{\mathrm{W}}^2+m_{\mathrm{Z}}^2) - 6b(m_{\mathrm{W}}^2+m_{\mathrm{Z}}^2) - 6b^2m_{\mathrm{W}}^2),\\
\boldsymbol{\delta_\epsilon\kappa_3} &= -\frac{\Delta_\epsilon}{16\pi^2}\frac{1}{2m_{\mathrm{H}}^2v^2}(\kappa_3(a^2-b+9\kappa_3^2-6\kappa_4)m_{\mathrm{H}}^4 - 3(1-a^2)\kappa_3m_{\mathrm{H}}^2(m_{\mathrm{W}}^2+m_{\mathrm{Z}}^2)),
\end{aligned}
$$

$$\boldsymbol{\delta_\epsilon a_{dd\mathcal{V}\mathcal{V}1}} = -\frac{\Delta_\epsilon}{16\pi^2}\frac{a^4+a^2b+b^2}{3}, \qquad \boldsymbol{\delta_\epsilon a_{dd\mathcal{V}\mathcal{V}2}} = -\frac{\Delta_\epsilon}{16\pi^2}\frac{(a^2-b)(2a^2+b+6)}{12},$$
$$\delta_\epsilon a_{11} = \frac{\Delta_\epsilon}{16\pi^2}\frac{a^2}{4}, \qquad \delta_\epsilon a_{H11} = \frac{\Delta_\epsilon}{16\pi^2}\frac{a(a^2-b)}{2}, \qquad \boldsymbol{\delta_\epsilon a_{HH11}} = \frac{\Delta_\epsilon}{16\pi^2}\frac{4a^4-5a^2b+b^2}{4},$$
$$\delta_\epsilon a_{HWW} = \frac{\Delta_\epsilon}{16\pi^2}\frac{a(a^2-b)}{12}, \qquad \boldsymbol{\delta_\epsilon a_{HHWW}} = -\frac{\Delta_\epsilon}{16\pi^2}\frac{4a^4-5a^2b+b^2}{24},$$
$$\delta_\epsilon a_{d2} = -\frac{\Delta_\epsilon}{16\pi^2}\frac{a(a^2-b)}{6}, \qquad \boldsymbol{\delta_\epsilon a_{Hd2}} = \frac{\Delta_\epsilon}{16\pi^2}\frac{4a^4-5a^2b+b^2}{6},$$
$$\delta_\epsilon a_{\Box\mathcal{V}\mathcal{V}} = -\frac{\Delta_\epsilon}{16\pi^2}\frac{a(2+a^2)}{4}, \qquad \boldsymbol{\delta_\epsilon a_{H\Box\mathcal{V}\mathcal{V}}} = \frac{\Delta_\epsilon}{16\pi^2}\frac{4a^4+a^2(4-3b)-2b}{4},$$
$$\delta_\epsilon a_{d3} = \frac{\Delta_\epsilon}{16\pi^2}\frac{a(a^2+b)}{2}, \qquad \boldsymbol{\delta_\epsilon a_{Hd3}} = \frac{\Delta_\epsilon}{16\pi^2}\frac{-4a^4+a^2b+b^2}{2},$$
$$\delta_\epsilon a_{\Box\Box} = -\frac{\Delta_\epsilon}{16\pi^2}\frac{3a^2}{4}, \qquad \boldsymbol{\delta_\epsilon a_{H\Box\Box}} = \frac{\Delta_\epsilon}{16\pi^2}\frac{3a(2a^2-b)}{2},$$
$$\boldsymbol{\delta_\epsilon a_{dd\Box}} = \frac{\Delta_\epsilon}{16\pi^2}\frac{3a(a^2-b)}{2}, \qquad \boldsymbol{\delta_\epsilon a_{Hdd}} = 0, \qquad \boldsymbol{\delta_\epsilon a_{ddW}}/2 = \boldsymbol{\delta_\epsilon a_{ddZ}} = -\frac{\Delta_\epsilon}{16\pi^2}3a(a^2-b),$$
$$\boldsymbol{\delta_\epsilon a_{H\mathcal{V}\mathcal{V}}} = \boldsymbol{\delta_\epsilon a_{HH\mathcal{V}\mathcal{V}}} = 0, \tag{4.14}$$

where we have used the **bold** notation for the new EChL coefficients in this computation with respect to Ref. [3]. As is expected from the $SU(2)_L \times U(1)_Y$ gauge-invariant construction of $\mathcal{L}_4$, we have found no ξ dependence in any of the CTs of the EChL coefficients (in contrast to the results for the CTs of the EW parameters, like δg, etc., that are in general ξ dependent; see Ref. [3]). We also see in these results that some of these CTs vanish for the choice $a = b = \kappa_3 = \kappa_4 = 1$, and others do not, like $a_{dd\mathcal{V}\mathcal{V}1}$, $a_{dd\mathcal{V}\mathcal{V}2}$, a_{11}, $a_{\Box\mathcal{V}\mathcal{V}}$, $a_{H\Box\mathcal{V}\mathcal{V}}$, a_{d3}, a_{Hd3}, $a_{\Box\Box}$, and $a_{H\Box\Box}$.

Some comments about the previous results in Eq. (4.14) are in order. First, we wish to note that these results, to our knowledge, are the only ones within the EChL that apply to the most general and complete renormalization program of off-shell, one-loop 1PI functions while including all types of bosonic loop diagrams in the R_ξ gauges. However, it is pertinent to compare our results with some previous results of the EChL one-loop divergences and counterterms in the literature. We will summarize this comparison as follows: First, we compare with previous works that compute the one-loop scattering amplitude. The renormalization of the $W_L W_L \to HH$ process was studied to one loop within the EChL previously in Ref. [4]. It was done by means of the ET—i.e., replacing the external W_L's with the w GBs and studying the corresponding $ww \to HH$ scattering with just chiral loops (meaning loops with only GBs and Higgs in the internal propagators), and assuming massless GBs (as in the Landau gauge, i.e., for $\xi = 0$). More recently, in Ref. [5], the loop contributions to the $W_L W_L \to HH$ scattering amplitude were computed as well by means of the ET—i.e., also for $ww \to HH$ scattering, but improving upon the previous computation of Ref. [4] by considering all kinds of bosonic one-loop diagrams in this scattering of GBs. They also used the Landau gauge—i.e., with massless GBs—and they simplify the computation by assuming the so-called isospin limit with $m_{\mathrm{W}} = m_{\mathrm{Z}}$. We have further improved these two computations in several aspects. We do not use the ET—i.e., we consider gauge bosons in the external legs, we work in generic R_ξ gauges (i.e., with massive GBs), and we do not work in the isospin limit—i.e., for us m_{W} and m_{Z} are different, as they correspond to the physical on-shell gauge boson masses. Furthermore, we consider the full set of 1PI functions involved in the amplitude and include all kinds of diagrams in those functions. The full set of one-loop diagrams computed here are in consequence different than in Ref. [5]. However, we can make contact with some of its results by specifying our results for the particular assumptions and approximations of that reference. For instance, taking into account the differences in the conventions, and setting $m_{\mathrm{Z}} = m_{\mathrm{W}}$, we find agreement for the CTs of a, b, λ, κ_3, and a_{d2}. On the other hand, to compare with this reference, it is convenient to use the reduced set of NLO coefficients that, as explained in the previous sections, can be obtained by the use of the equations of motion. Concretely, the EChL NLO coefficients appearing in the scattering amplitude are those presented in Eq. (3.17), and they appear within the particular combinations of coefficients given in Eq. (2.13). Therefore, these are the ones that should be compared with Ref. [5]. From our results in Eq. (4.14), our prediction for the divergences of these combinations are

$$\delta_\epsilon \eta = \delta_\epsilon \tilde{a}_{dd\mathcal{V}\mathcal{V}1} = \delta_\epsilon(a_{dd\mathcal{V}\mathcal{V}1} - 4a^2 a_{11} + 2a a_{d3}) = -\frac{\Delta_\epsilon}{16\pi^2}\frac{(a^2-b)^2}{3},$$
$$\delta_\epsilon \delta = \delta_\epsilon \tilde{a}_{dd\mathcal{V}\mathcal{V}2} = \delta_\epsilon\left(a_{dd\mathcal{V}\mathcal{V}2} + \frac{a}{2}a_{dd\Box}\right) = \frac{\Delta_\epsilon}{16\pi^2}\frac{(a^2-b)(7a^2-b-6)}{12},$$
$$\delta_\epsilon(a_{H\mathcal{V}\mathcal{V}} - 2a_{\Box\mathcal{V}\mathcal{V}} + 2a a_{\Box\Box}) = \frac{\Delta_\epsilon}{16\pi^2}a(1-a^2),$$
$$\delta_\epsilon(a_{HH\mathcal{V}\mathcal{V}} - 6\kappa_3 a_{\Box\mathcal{V}\mathcal{V}} - 4a_{H\Box\mathcal{V}\mathcal{V}} + 4b a_{\Box\Box} + 6\kappa_3 a a_{\Box\Box} + 4a a_{H\Box\Box}) = \frac{\Delta_\epsilon}{16\pi^2}(3\kappa_3 a(1-a^2) + 2b - 2a^2(2+3b) + 8a^4),$$
$$\delta_\epsilon(a_{Hdd} - a_{dd\Box}) = -\frac{\Delta_\epsilon}{16\pi^2}\frac{3a(a^2-b)}{2}. \tag{4.15}$$

The first two lines in the above equation are in agreement with the result for η and δ in Refs. [4,5], where a_{11}, a_{d3}, and $a_{dd\Box}$ were not considered. It is interesting to remark that the combinations in Eq. (4.15) indeed vanish for $a = b = \kappa_3 = 1$, as expected in the comparison with the SM.

Second, we compare our results with Ref. [6]. In this work, the renormalization of one-loop 1PI functions was performed for off-shell external legs, but they considered the pure scalar theory—i.e., only the Higgs and GBs sector of the EChL—and worked with massless GBs (as in the Landau gauge, with $\xi = 0$). No gauge or ghost fields were included, and therefore no gauge-fixing. We find agreement in the divergences found for the subset of a_i's involved in the scalar sector (the coefficients in the notation of Ref. [6] are specified inside the parentheses). Concretely, we agree in a (a_C), b (b_C), κ_3 (μ_3), $a_{dd\mathcal{V}\mathcal{V}1}$ (c_8), $a_{dd\mathcal{V}\mathcal{V}2}$ (c_{20}), a_{11} (c_9), a_{H11} (a_9), a_{HH11} (b_9), $a_{dd\Box}$ ($c_{\Delta H}$), $a_{\Box\mathcal{V}\mathcal{V}}$ (c_7), $a_{H\Box\mathcal{V}\mathcal{V}}$ (a_7), a_{d3} (c_{10}), a_{Hd3} (a_{10}), $a_{\Box\Box}$ ($c_{\Box H}$), and $a_{H\Box\Box}$ ($a_{\Box H}$).

Third, we compare our results with others that do not study scattering amplitudes but are devoted to the renormalization of the Lagrangian. In particular, the renormalization of the EChL was studied in the path integral formalism, using the background field method, in Refs. [7,21,22]. The most complete comparison of our results should be performed with the bosonic loop results of Refs. [7,22], since these also included all loops of scalar and gauge particles. However, the comparison with the path integral results is tricky, since they use the equations of motion to reduce the number of operators in the Lagrangian. Therefore, some off-shell divergences do not appear in their results, and some others are redefined by the use of the equations of motion. They also use redefinitions of the fields (in particular, the Higgs field) to reach the canonical kinetic term in the Lagrangian. On the other hand, the parametrization used in Refs. [7,22] is also very different from that used here and is not straightforward to compare with. For example, the divergence canceled by our a_{ddW}, a_{ddZ}, and a_{Hdd} in the HHH Green's function is absorbed via the Higgs field redefinition in their context.

Finally, we summarize in the following the main results regarding the renormalization group running equations (RGEs) for the NLO EChL coefficients, which complement those given in our previous work [3]. These RGEs can be easily derived from the previous results in Eq. (4.14) and taking into account the relation between the renormalized and bare coefficients given by $a_i^0 = a_i + \delta a_i$. In the $\overline{\text{MS}}$ scheme (with μ being the scale of dimensional regularization in $D = 4 - \epsilon$ dimensions), the running $a_i(\mu)$ can be written as follows:

$$a_i(\mu) = a_i^0 - \delta a_i(\mu), \qquad \delta a_i(\mu) = \delta_\epsilon a_i - \frac{\gamma_{a_i}}{16\pi^2}\log\mu^2,$$
$$\delta_\epsilon a_i = \frac{\Delta_\epsilon}{16\pi^2}\gamma_{a_i}, \tag{4.16}$$

where the divergent $\delta_\epsilon a_i$ is written in terms of the anomalous dimension γ_{a_i} of the corresponding effective operator. The running and renormalized a_i's can then be related, in practice, by

$$a_i(\mu) = a_i + \frac{\gamma_{a_i}}{16\pi^2}\log\mu^2. \tag{4.17}$$

The set of RGEs for all the a_i's then immediately follows:

$$a_i(\mu) = a_i(\mu') + \frac{1}{16\pi^2}\gamma_{a_i}\log\left(\frac{\mu^2}{\mu'^2}\right), \tag{4.18}$$

where the specific value of γ_{a_i} for each coefficient can be read from Eq. (4.14). For instance, in the case of the two most relevant NLO-EChL coefficients for the present $WW \to HH$ scattering, η and δ, we get the following RGEs:

$$\eta(\mu) = \eta(\mu') - \frac{1}{16\pi^2}\frac{1}{3}(a^2-b)^2\log\left(\frac{\mu^2}{\mu'^2}\right),$$
$$\delta(\mu) = \delta(\mu') + \frac{1}{16\pi^2}\frac{1}{12}(a^2-b)(7a^2-b-6)\log\left(\frac{\mu^2}{\mu'^2}\right), \tag{4.19}$$

which are in agreement with the RGEs given in Ref. [4]. Notice that, in particular for $a = b = 1$, these two EChL coefficients η and δ do not run; therefore, they are RGE invariants.

V. NUMERICAL RESULTS FOR $W_L^+W_L^- \to HH$

In this section, we study the numerical predictions from the EChL for the cross section of the scattering process $WW \to HH$ and compare the tree-level rates with the one-loop rates. We also compare these rates with the SM case which have been computed independently here following the same procedure as for the EChL case. It is also interesting to compare this SM case with previous SM results in the literature [23]. Since, as we have already said, the dominant contribution to this scattering process in the TeV domain is that coming from the longitudinally polarized gauge boson modes, we will focus in this section on this most relevant cross section—i.e., on $\sigma(W_L^+W_L^- \to HH)$. In addition, this numerical study of the radiative corrections will be devoted to the most relevant coefficients of the NLO-EChL, which, as already said, are the parameters η and δ. For simplicity, the LO-EChL parameters will be set here to the SM default values—i.e., in the following we set $a = b = \kappa_3 = \kappa_4 = 1$. All the numerical computations presented here have been

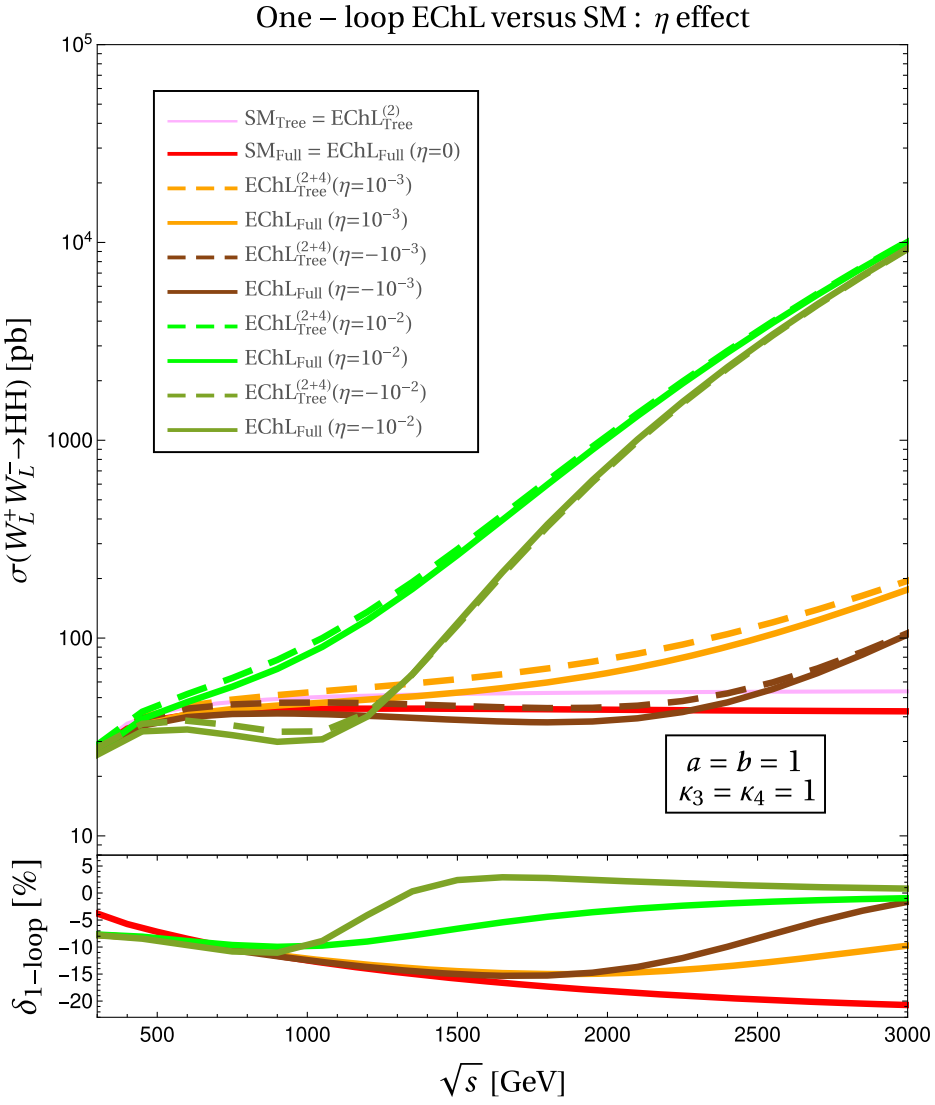

FIG. 4. Cross section prediction for $W_L^+W_L^- \to HH$ as a function of the energy $\sqrt{s}$ within the EChL at one-loop level (solid lines) and comparison with the tree-level prediction (dashed lines). The effect of the NLO parameter η is displayed, assuming values for this parameter of $\pm 10^{-2}$ and $\pm 10^{-3}$. The LO parameters are set to $a = b = \kappa_3 = \kappa_4 = 1$. The other NLO parameters are set to zero. The SM predictions at tree level (pink) and one-loop level (red) are also included. The relative size of the one-loop prediction with respect to the tree-level prediction, defined by means of $\delta_{1\text{-loop}}$ in Eq. (5.1), is displayed at the bottom of this figure. The color code is red (SM), orange (EChL, $\eta = 10^{-3}$), brown (EChL, $\eta = -10^{-3}$), bright green (EChL, $\eta = 10^{-2}$), and green (EChL, $\eta = -10^{-2}$).

performed with the help of FormCalc and LoopTools, and for definiteness, we choose the Feynman–'t Hooft gauge—i.e., we fix $\xi = 1$.

First of all, it is worth mentioning that we have done a numerical check of the finiteness of the predicted one-loop cross section in both cases, the EChL and the SM. This is done indirectly, by checking numerically the renormalization μ-scale independence of the result. This is not a trivial check at all, since the computation of the one-loop amplitude from the 1PI functions amounts to the evaluation of more than 500 one-loop diagrams, where each one depends on this μ scale. Thus, the cancellation of the μ dependence among the various diagrams found in the final result is a quite convincing check. Notice that for the studied case here of $a = b = 1$, the two parameters δ and η, as already said, do not run; therefore, they have equal value at any assumed μ scale.

We next summarize our numerical results for $\sigma(W_L^+W_L^- \to HH)$ as a function of the center-of-mass energy $\sqrt{s}$ in the two Figs. 4 and 5. In Fig. 4, we study the effect of η, and in Fig. 5, we study the effect of δ. In both cases, we have explored the following values for those coefficients, ± 0.01 and ± 0.001, which are allowed by present experimental data. In both plots we have included, for comparison, the following rates: (i) the tree level predictions for the EChL, $\text{EChL}_{\text{Tree}}^{(2+4)}$; (ii) the full one-loop

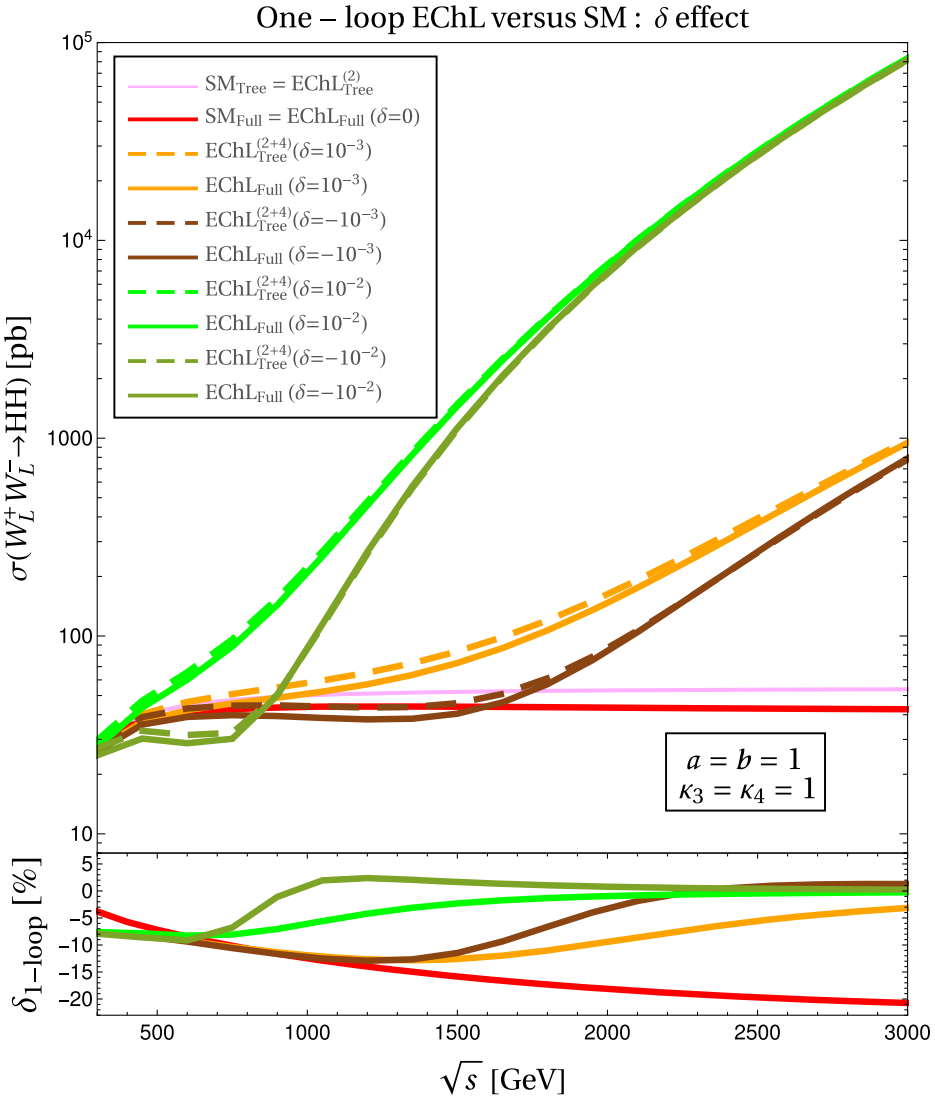

FIG. 5. Cross section prediction for $W_L^+W_L^- \to HH$ as a function of the energy $\sqrt{s}$ within the EChL at one-loop level (solid lines) and comparison with the tree-level prediction (dashed lines). The effect of the NLO parameter δ is displayed, assuming values for this parameter of $\pm 10^{-2}$ and $\pm 10^{-3}$. The LO parameters are set to $a = b = \kappa_3 = \kappa_4 = 1$. The other NLO parameters are set to zero. The SM predictions at tree level (pink) and one-loop level (red) are also included. The relative size of the one-loop prediction with respect to the tree-level prediction, defined by means of $\delta_{\text{1-loop}}$ in Eq. (5.1), is displayed at the bottom of this figure. The color code is red (SM), orange (EChL, $\delta = 10^{-3}$), brown (EChL, $\delta = -10^{-3}$), bright green (EChL, $\delta = 10^{-2}$), and green (EChL, $\delta = -10^{-2}$).

predictions for the EChL, $\mathrm{EChL}_{\mathrm{Full}}$; (iii) the tree level predictions for the SM, $\mathrm{SM}_{\mathrm{Tree}}$ (which coincides with the LO result in the EChL, $\mathrm{EChL}^{(2)}_{\mathrm{Tree}}$); and (iv) the full one-loop predictions for the SM, $\mathrm{SM}_{\mathrm{Full}}$. In the lower parts of these plots, we display the predictions for the relative size of the one-loop correction with respect to the tree-level prediction, by means of $\delta_{\text{1-loop}}$, which is defined by

$$\delta_{\text{1-loop}} = \frac{(\sigma_{\mathrm{Full}} - \sigma_{\mathrm{Tree}})}{\sigma_{\mathrm{Tree}}}. \tag{5.1}$$

The main features learned from these two figures are the following:

(1) We get a one-loop correction in the SM case that is negative and increases in size with energy. The size of $\delta_{\text{1-loop}}$ can be up to $\sim -20\%$ at the maximum energy studied of $\sqrt{s} = 3$ TeV, and it is in accordance with Ref. [23].
(2) The predictions from the EChL, both at tree level and one-loop level, show a clear departure from the corresponding SM prediction. The largest deviations occur for the largest $|\delta|$ and/or $|\eta|$ considered values.
(3) We get a one-loop correction in the EChL case that can be either negative or positive depending on the value of the coefficient and the value of the energy. For η, we find it to be negative for $\pm 10^{-3}$ and $+10^{-2}$ at all the studied energies. But it is positive for -10^{-2} in the interval 1.3 TeV $< \sqrt{s} <$ 3 TeV. For δ, we find it to be negative for $+10^{-2}$ and $+10^{-3}$ at all the studied energies. But it is positive for -10^{-2} in the interval 0.9 TeV $< \sqrt{s} <$ 3 TeV and for -10^{-3} in the interval 2.5 TeV $< \sqrt{s} <$ 3 TeV.
(4) Overall, we see that the maximum size of the radiative one-loop correction found in the EChL is about -15% in both the η and δ cases. This is a bit lower than in the SM case.
(5) Finally, we notice that the values of the coefficients η and δ specified in these plots refer to the renormalized parameter values. However, since we have taken in these plots $a = b = 1$, they do not depend on the μ scale. This, together with the previously mentioned μ independence of the sum of all the contributing one-loop diagrams, complements the check of μ-scale invariance of the total cross section result.

VI. CONCLUSIONS

In this work, we have computed the one-loop electroweak radiative corrections to the scattering process $WW \to HH$ within the context of the Higgs effective field theory, considering that the new Higgs physics beyond the SM enters only in the bosonic sector, and it is given by the electroweak chiral Lagrangian. We consider this EChL with all the relevant effective operators of chiral dimensions two and four and present the computation in terms of the involved 1PI Green's functions in covariant R_ξ gauges. An ambitious renormalization program for all these one-loop 1PI functions involved is developed, considering the most general case with arbitrary momenta for the external particle legs. This renormalization procedure is more demanding than just requiring a finite result for the one-loop amplitude with external on-shell particles, and it has the advantage of being applicable to several processes sharing some of those 1PI functions with the amplitude under study here. We have applied this same procedure for both cases, the EChL and the SM. In particular, we have used here for $WW \to HH$ scattering some of the previous renormalized 1PI functions computed in our previous work devoted to $WZ \to WZ$ scattering. We have used those functions also here, and then we have complemented them with the new one-loop 1PI functions for the new vertices involving the Higgs particle, HHH, HWW, πWH, AHH, ZHH, and $WWHH$, whose results are presented here.

One of the most important results contained in this work is the full set of divergent counterterms derived for the EChL coefficients, summarized in Eqs. (4.14) and (4.15). This set of divergences also determines the corresponding set of RGEs for the involved HEFT coefficients, according to Eqs. (4.16)–(4.19). A small subset of these results have been cross-checked with previous results in the literature which were found following a very different approach to ours, and we have found agreement with these. A discussion on this comparison has also been included in the present work.

The final part of this paper has been devoted to the numerical computation of the one-loop radiative corrections to the cross section of the $W_L W_L \to HH$ scattering process. Again, we have done in parallel both the computation for the EChL and that for the SM. In the case of the SM, we have found agreement with the previous result in Ref. [23]. Our estimate of the one-loop correction with respect to the tree-level cross section in the SM gives a negative value whose maximum size is reached at the largest energy studied of $\sqrt{s} = 3$ TeV and is about $\delta_{\text{1-loop}} \sim -20\%$. In the EChL case, where we have considered the effects from the two most relevant parameters η and δ, we find also important one-loop corrections, with a maximum of about $\delta_{\text{1-loop}} \sim -15\%$, a bit lower than in the SM case. The size of this correction depends on the energy and the particular values of the EChL coefficients. The largest departures of the HEFT with respect to the SM prediction are found for the largest studied values of δ and/or η. There are also some input values for these parameters and energy ranges that provide a positive one-loop correction, although small, being below 5%. All these numerical results are summarized in Figs. 4 and 5.

ACKNOWLEDGMENTS

We would like first to warmly thank Daniel Domenech for his valuable help in producing Fig. 3. The work of M. J. H. has received financial support from the "Spanish Agencia Estatal de Investigación" (AEI) and the EU

"Fondo Europeo de Desarrollo Regional" (FEDER) through Project No. PID2019-108892RB-I00/AEI/10.13039/501100011033 and from IFT Centro de Excelencia Severo Ochoa Grant No. SEV-2016-0597. We also acknowledge financial support from the European Union's Horizon 2020 research and innovation program under the Marie Sklodowska-Curie Grant Agreements No. 674896 and No. 860881-HIDDeN, the ITN ELUSIVES H2020-MSCA-ITN-2015//674896, and the RISE INVISIBLESPLUS H2020-MSCA-RISE-2015//690575. The work of R. M. is supported by CONICET and ANPCyT under Projects No. PICT 2016-0164, No. PICT 2017-2751, and No. PICT 2018-03682.

APPENDIX A: SUMMARY OF COMPLEMENTARY 1PI FUNCTIONS

For completeness, we summarize in this appendix the renormalized 1PI functions already derived in Ref. [3] that also enter into the present $WW \to HH$ scattering. We have taken these analytical results from that previous reference, but we have displayed them here by setting $\xi = 1$, as in the main results of this paper. The definition of the EChL coefficients, parameters, and functions entering into these complementary functions can be found in Ref. [3].

Starting with the EChL, the one-leg function (Higgs tadpole) is

$$i\hat{T} = iT^{\rm Loop} - i\delta T, \qquad \delta T = (\delta m_{\rm H}^2 - m_{\rm H}^2(-2\delta Z_H + \delta\lambda/\lambda + Z_\pi + 2\delta v/v))v. \tag{A1}$$

Notice that now we are fixing a typo in this counterterm with respect to our previous publication.

The two-leg functions are

$$\begin{aligned}
-i\hat{\Sigma}_{HH}(q^2) &= -i\Sigma_{HH}^{\rm Loop}(q^2) + i(\delta Z_H(q^2 - m_{\rm H}^2) - \delta m_{\rm H}^2) + i\frac{2a_{\Box\Box}}{v^2}q^4,\\
i\hat{\Sigma}_{WW}^{T}(q^2) &= i\Sigma_{WW}^{T\rm Loop}(q^2) - i(\delta Z_W(q^2 - m_{\rm W}^2) - \delta m_{\rm W}^2),\\
i\hat{\Sigma}_{WW}^{L}(q^2) &= i\Sigma_{WW}^{L\rm Loop}(q^2) + i(-(q^2 - m_{\rm W}^2)\delta Z_W + \delta m_{\rm W}^2 + q^2\delta\xi_1) - iq^2g^2a_{11},\\
\hat{\Sigma}_{W\pi}(q^2) &= \Sigma_{W\pi}^{\rm Loop}(q^2) + \frac{\delta\xi_2 - \delta\xi_1}{2}m_{\rm W}^2 + q^2g^2a_{11},\\
-i\hat{\Sigma}_{\pi\pi}(q^2) &= -i\Sigma_{\pi\pi}^{\rm Loop}(q^2) + i((q^2 - m_{\rm W}^2)\delta Z_\pi - \delta m_{\rm W}^2 - m_{\rm W}^2\delta\xi_2) - i\frac{g^2}{m_{\rm W}^2}q^4a_{11}.
\end{aligned} \tag{A2}$$

In these formulas above, the a_i coefficients must be understood again as $a_i + \delta a_i$.

On the other hand, the three-leg functions corresponding to $W^\mu(k_1)W^\nu(k_2)V^\rho(q)$ (with $V = A, Z$) enter into the present work just at the LO; therefore, they take the usual tree-level expression:

$$\begin{aligned}
i\Gamma_{W^+W^-A}^{\mu\nu\rho} &= -igs_{\rm w}(g^{\mu\nu}(k_1 - k_2)^\rho + g^{\nu\rho}(k_2 - q)^\mu + g^{\rho\mu}(q - k_1)^\nu),\\
i\Gamma_{W^+W^-Z}^{\mu\nu\rho} &= -igc_{\rm w}(g^{\mu\nu}(k_1 - k_2)^\rho + g^{\nu\rho}(k_2 - q)^\mu + g^{\rho\mu}(q - k_1)^\nu).
\end{aligned} \tag{A3}$$

In contrast, the AHH and ZHH 1PI functions in the second diagram of Fig. 1 vanish at LO, and they get only NLO contributions that are finite.

Next, we summarize the loop divergences of all the above 1PI functions. These are

$$\begin{aligned}
iT^{\rm Loop}|_{\rm div} &= i\frac{\Delta_\epsilon}{16\pi^2}\frac{3}{2v}(\kappa_3 m_{\rm H}^4 + 2a(2m_{\rm W}^4 + m_{\rm Z}^4)),\\
-i\Sigma_{HH}^{\rm Loop}(q^2)|_{\rm div} &= i\frac{\Delta_\epsilon}{16\pi^2}\frac{3}{2v^2}(a^2q^4 - 2a^2(2m_{\rm W}^2 + m_{\rm Z}^2)q^2 + (3\kappa_3^2 + \kappa_4)m_{\rm H}^4 + (4a^2 + 2b)(2m_{\rm W}^4 + m_{\rm Z}^4)),\\
i\Sigma_{WW}^{T\rm Loop}(q^2)|_{\rm div} &= i\frac{\Delta_\epsilon}{16\pi^2}\frac{g^2}{12}((39 - a^2)q^2 + 3(a^2 - b)m_{\rm H}^2 + 3(13 - 3a^2)m_{\rm W}^2 - 9m_{\rm Z}^2),\\
i\Sigma_{WW}^{L\rm Loop}(q^2)|_{\rm div} &= i\frac{\Delta_\epsilon}{16\pi^2}\frac{g^2}{4}(a^2q^2 + (a^2 - b)m_{\rm H}^2 + (13 - 3a^2)m_{\rm W}^2 - 3m_{\rm Z}^2),\\
i\Sigma_{W\pi}^{\rm Loop}(q^2)|_{\rm div} &= i\frac{\Delta_\epsilon}{16\pi^2}\frac{g^2}{4}(-a^2q^2 - (a^2 - b)m_{\rm H}^2 - (17/3 - 3a^2)m_{\rm W}^2 + (7/3)m_{\rm Z}^2),\\
-i\Sigma_{\pi\pi}^{\rm Loop}(q^2)|_{\rm div} &= i\frac{\Delta_\epsilon}{16\pi^2}\left(\frac{a^2}{v^2}q^4 + \frac{q^2}{v^2}((a^2 - b)m_{\rm H}^2 - (5/3 + 3a^2)m_{\rm W}^2 - (5/3)m_{\rm Z}^2)\right).
\end{aligned} \tag{A4}$$

The resulting divergent part of the EChL counterterms for the EW parameters was also derived in Ref. [3]. We include those results here, including now explicitly $\delta_\epsilon\lambda$, setting $\xi = 1$:

$$
\begin{aligned}
\delta_\epsilon Z_H &= \frac{\Delta_\epsilon}{16\pi^2}\frac{3a^2}{v^2}(2m_{\rm W}^2 + m_{\rm Z}^2), \qquad \delta_\epsilon T = \frac{\Delta_\epsilon}{16\pi^2}\frac{3}{2v}(\kappa_3 m_{\rm H}^4 + 2a(2m_{\rm W}^4 + m_{\rm Z}^4)),\\
\delta_\epsilon m_{\rm H}^2 &= \frac{\Delta_\epsilon}{16\pi^2}\frac{3}{2v^2}((3\kappa_3^2 + \kappa_4)m_{\rm H}^4 - 2a^2 m_{\rm H}^2(2m_{\rm W}^2 + m_{\rm Z}^2) + (4a^2 + 2b)(2m_{\rm W}^4 + m_{\rm Z}^4)),\\
\delta_\epsilon Z_B &= -\frac{\Delta_\epsilon}{16\pi^2}\frac{g'^2}{12}(1 + a^2), \qquad \delta_\epsilon Z_W = \frac{\Delta_\epsilon}{16\pi^2}\frac{g^2}{12}(39 - a^2),\\
\delta_\epsilon m_{\rm W}^2 &= -\frac{\Delta_\epsilon}{16\pi^2}\frac{g^2}{12}(3(a^2 - b)m_{\rm H}^2 + (78 - 10a^2)m_{\rm W}^2 - 9m_{\rm Z}^2),\\
\delta_\epsilon m_{\rm Z}^2 &= \frac{\Delta_\epsilon}{16\pi^2}\frac{g^2}{12c_{\rm w}^2}(-3(a^2 - b)m_{\rm H}^2 + (7(1 + a^2) + 2(-43 + a^2)c_{\rm w}^2)m_{\rm W}^2 + (10 + a^2)m_{\rm Z}^2),\\
\delta_\epsilon g'/g' &= 0, \qquad \delta_\epsilon g/g = -\frac{\Delta_\epsilon}{16\pi^2}2g^2,\\
\delta_\epsilon \xi_1 &= \frac{\Delta_\epsilon}{16\pi^2}\frac{g^2}{12}(39 - a^2),\\
\delta_\epsilon \xi_2 &= \frac{\Delta_\epsilon}{16\pi^2}\frac{1}{3v^2}(6(a^2 - b)m_{\rm H}^2 + (73 - 19a^2)m_{\rm W}^2 - 14m_{\rm Z}^2),\\
\delta_\epsilon Z_\pi &= -\frac{\Delta_\epsilon}{16\pi^2}\frac{1}{v^2}((a^2 - b)m_{\rm H}^2 - (5/3 + 3a^2)m_{\rm W}^2 - (5/3)m_{\rm Z}^2),\\
\delta_\epsilon v/v &= \frac{\Delta_\epsilon}{16\pi^2}\frac{2(m_{\rm W}^2 + m_{\rm Z}^2)}{3v^2},\\
\delta_\epsilon \lambda &= \frac{\Delta_\epsilon}{16\pi^2}\frac{1}{4v^4}(2a^2(m_{\rm H}^4 + 3m_{\rm H}^2(m_{\rm W}^2 + m_{\rm Z}^2) + 6(2m_{\rm W}^4 + m_{\rm Z}^4)) - 6a(2m_{\rm W}^4 + m_{\rm Z}^4)\\
&\quad -2b(m_{\rm H}^4 - 3(2m_{\rm W}^4 + m_{\rm Z}^4)) + 3(3\kappa_3^2 - \kappa_3 m_{\rm H}^4 + \kappa_4)m_{\rm H}^4 - 6m_{\rm H}^2(m_{\rm W}^2 + m_{\rm Z}^2)).
\end{aligned}
\tag{A5}
$$

Finally, the corresponding results in the SM with $\xi = 1$ are

$$
\begin{aligned}
i\hat{\bar{T}} &= i\bar{T}^{\rm Loop} - i\delta\bar{T}, \qquad \delta\bar{T} = (\delta m_{\rm H}^2 - m_{\rm H}^2(-\delta Z_\phi + \delta\lambda/\lambda + 2\delta v/v))v,\\
-i\hat{\bar{\Sigma}}_{HH}(q^2) &= -i\bar{\Sigma}_{HH}^{\rm Loop}(q^2) + i(\delta Z_\phi(q^2 - m_{\rm H}^2) - \delta m_{\rm H}^2),\\
i\hat{\bar{\Sigma}}_{WW}^{T}(q^2) &= i\bar{\Sigma}_{WW}^{T\rm Loop}(q^2) - i(\delta Z_W(q^2 - m_{\rm W}^2) - \delta m_{\rm W}^2),\\
i\hat{\bar{\Sigma}}_{WW}^{L}(q^2) &= i\bar{\Sigma}_{WW}^{L\rm Loop}(q^2) + i(-(q^2 - m_{\rm W}^2)\delta Z_W + \delta m_{\rm W}^2 + q^2\delta\xi_1),\\
\hat{\bar{\Sigma}}_{W\pi}(q^2) &= \bar{\Sigma}_{W\pi}^{\rm Loop}(q^2) + \frac{\delta\xi_2 - \delta\xi_1}{2}m_{\rm W}^2,\\
-i\hat{\bar{\Sigma}}_{\pi\pi}(q^2) &= -i\bar{\Sigma}_{\pi\pi}^{\rm Loop}(q^2) + i((q^2 - m_{\rm W}^2)\delta Z_\phi - \delta m_{\rm W}^2 - m_{\rm W}^2\delta\xi_2 - \delta\bar{T}/v),
\end{aligned}
\tag{A6}
$$

and again the WWA and the WWZ vertices enter only at the tree level in this amplitude, therefore

$$
\begin{aligned}
i\bar{\Gamma}_{W^+W^-A}^{\mu\nu\rho} &= -igs_{\rm w}(g^{\mu\nu}(k_1 - k_2)^\rho + g^{\nu\rho}(k_2 - q)^\mu + g^{\rho\mu}(q - k_1)^\nu),\\
i\bar{\Gamma}_{W^+W^-Z}^{\mu\nu\rho} &= -igc_{\rm w}(g^{\mu\nu}(k_1 - k_2)^\rho + g^{\nu\rho}(k_2 - q)^\mu + g^{\rho\mu}(q - k_1)^\nu),
\end{aligned}
\tag{A7}
$$

whereas the AHH and ZHH vertices vanish at the tree level, and these 1PI functions only get one-loop corrections that are finite.

The loop divergences of the above 1PI functions in the SM are

$$
\begin{aligned}
i\bar{T}^{\mathrm{Loop}}|_{\mathrm{div}} &= i\frac{\Delta_\epsilon}{16\pi^2}\frac{1}{2v}(3m_{\mathrm{H}}^4+6(2m_{\mathrm{W}}^4+m_{\mathrm{Z}}^4)+m_{\mathrm{H}}^2(2m_{\mathrm{W}}^2+m_{\mathrm{Z}}^2)),\\
-i\bar{\Sigma}_{HH}^{\mathrm{Loop}}(q^2)|_{\mathrm{div}} &= i\frac{\Delta_\epsilon}{16\pi^2}\frac{1}{2v^2}(-4(2m_{\mathrm{W}}^2+m_{\mathrm{Z}}^2)q^2+15m_{\mathrm{H}}^4+18(2m_{\mathrm{W}}^4+m_{\mathrm{Z}}^4)+m_{\mathrm{H}}^2(2m_{\mathrm{W}}^2+m_{\mathrm{Z}}^2)),\\
i\bar{\Sigma}_{WW}^{T\mathrm{Loop}}(q^2)|_{\mathrm{div}} &= i\frac{\Delta_\epsilon}{16\pi^2}\frac{g^2}{6}(19q^2+6(2m_{\mathrm{W}}^2-m_{\mathrm{Z}}^2)),\\
i\bar{\Sigma}_{WW}^{L\mathrm{Loop}}(q^2)|_{\mathrm{div}} &= i\frac{\Delta_\epsilon}{16\pi^2}g^2(2m_{\mathrm{W}}^2-m_{\mathrm{Z}}^2),\\
i\bar{\Sigma}_{W\pi}^{\mathrm{Loop}}(q^2)|_{\mathrm{div}} &= i\frac{\Delta_\epsilon}{16\pi^2}\frac{g^2}{4}(-2m_{\mathrm{W}}^2+3m_{\mathrm{Z}}^2),\\
-i\bar{\Sigma}_{\pi\pi}^{\mathrm{Loop}}(q^2)|_{\mathrm{div}} &= i\frac{\Delta_\epsilon}{16\pi^2}\frac{g^2}{2}(-4(2m_{\mathrm{W}}^2+m_{\mathrm{Z}}^2)q^2+3m_{\mathrm{H}}^4+12m_{\mathrm{W}}^4+6m_{\mathrm{Z}}^4+m_{\mathrm{H}}^2(2m_{\mathrm{W}}^2+m_{\mathrm{Z}}^2)),
\end{aligned}
\tag{A8}
$$

and the resulting divergences of the counterterms are

$$
\begin{aligned}
\delta_\epsilon Z_\phi &= \frac{\Delta_\epsilon}{16\pi^2}\frac{2}{v^2}(2m_{\mathrm{W}}^2+m_{\mathrm{Z}}^2), \qquad \delta_\epsilon\bar{T} = \frac{\Delta_\epsilon}{16\pi^2}\frac{1}{2v}(3m_{\mathrm{H}}^4+6(2m_{\mathrm{W}}^4+m_{\mathrm{Z}}^4)+m_{\mathrm{H}}^2(2m_{\mathrm{W}}^2+m_{\mathrm{Z}}^2)),\\
\delta_\epsilon m_{\mathrm{H}}^2 &= \frac{\Delta_\epsilon}{16\pi^2}\frac{3}{2v^2}(5m_{\mathrm{H}}^4-m_{\mathrm{H}}^2(2m_{\mathrm{W}}^2+m_{\mathrm{Z}}^2)+6(2m_{\mathrm{W}}^4+m_{\mathrm{Z}}^4)),\\
\delta_\epsilon Z_B &= -\frac{\Delta_\epsilon}{16\pi^2}\frac{g'^2}{6}, \qquad \delta_\epsilon Z_W = \frac{\Delta_\epsilon}{16\pi^2}\frac{19g^2}{6},\\
\delta_\epsilon m_{\mathrm{W}}^2 &= -\frac{\Delta_\epsilon}{16\pi^2}\frac{g^2}{6}(31m_{\mathrm{W}}^2-6m_{\mathrm{Z}}^2),\\
\delta_\epsilon m_{\mathrm{Z}}^2 &= \frac{\Delta_\epsilon}{16\pi^2}\frac{g^2}{6c_{\mathrm{w}}^2}((10-42c_{\mathrm{w}}^2)m_{\mathrm{W}}^2+7m_{\mathrm{Z}}^2),\\
\delta_\epsilon g'/g' &= 0, \qquad \delta_\epsilon g/g = -\frac{\Delta_\epsilon}{16\pi^2}2g^2,\\
\delta_\epsilon\xi_1 &= \frac{\Delta_\epsilon}{16\pi^2}\frac{19g^2}{6}, \qquad \delta_\epsilon\xi_2 = \frac{\Delta_\epsilon}{16\pi^2}\frac{2}{3v^2}(25m_{\mathrm{W}}^2-9m_{\mathrm{Z}}^2),\\
\delta_\epsilon v/v &= \frac{\Delta_\epsilon}{16\pi^2}\frac{2m_{\mathrm{W}}^2+m_{\mathrm{Z}}^2}{v^2},\\
\delta_\epsilon\lambda &= \frac{\Delta_\epsilon}{16\pi^2}\frac{1}{v^4}(3m_{\mathrm{H}}^4-m_{\mathrm{H}}^2(2m_{\mathrm{W}}^2+m_{\mathrm{Z}}^2)+3(2m_{\mathrm{W}}^4+m_{\mathrm{Z}}^4)).
\end{aligned}
\tag{A9}
$$

APPENDIX B: RELEVANT ONE-LOOP DIAGRAMS

In this appendix, we present the relevant one-loop diagrams entering into the computation of the 1PI functions for $WW \to HH$ scattering within the EChL. In particular, we give the corresponding diagrams to the new Green's functions, Γ_{HHH}, $\Gamma_{\pi WH}$, Γ_{AHH}, Γ_{ZHH}, and Γ_{WWHH}, with respect to our previous computation in Ref. [3]. These diagrams were generated with FeynArts [15], and we collect them by different topologies using a generic notation for the internal propagators: dashed lines refer to either Higgs bosons or Goldstone bosons, and wavy lines refer to all possible EW gauge bosons. Notice the absence of ghost fields, since the Higgs boson does not interact with them in the EChL, but they are present in the SM computation.

The loop diagrams of Γ_{HHH} are shown in the first column of Fig. 6. Differently from the SM, the results in the EChL depend on a, b, κ_3, and κ_4, and there is a different (nontrivial) momentum dependence due to the behavior of the scalar loop diagrams in the EChL and the SM. The same conclusions apply for the diagrams in the second column corresponding to $\Gamma_{\pi WH}$, but there is no κ_4 dependence here.

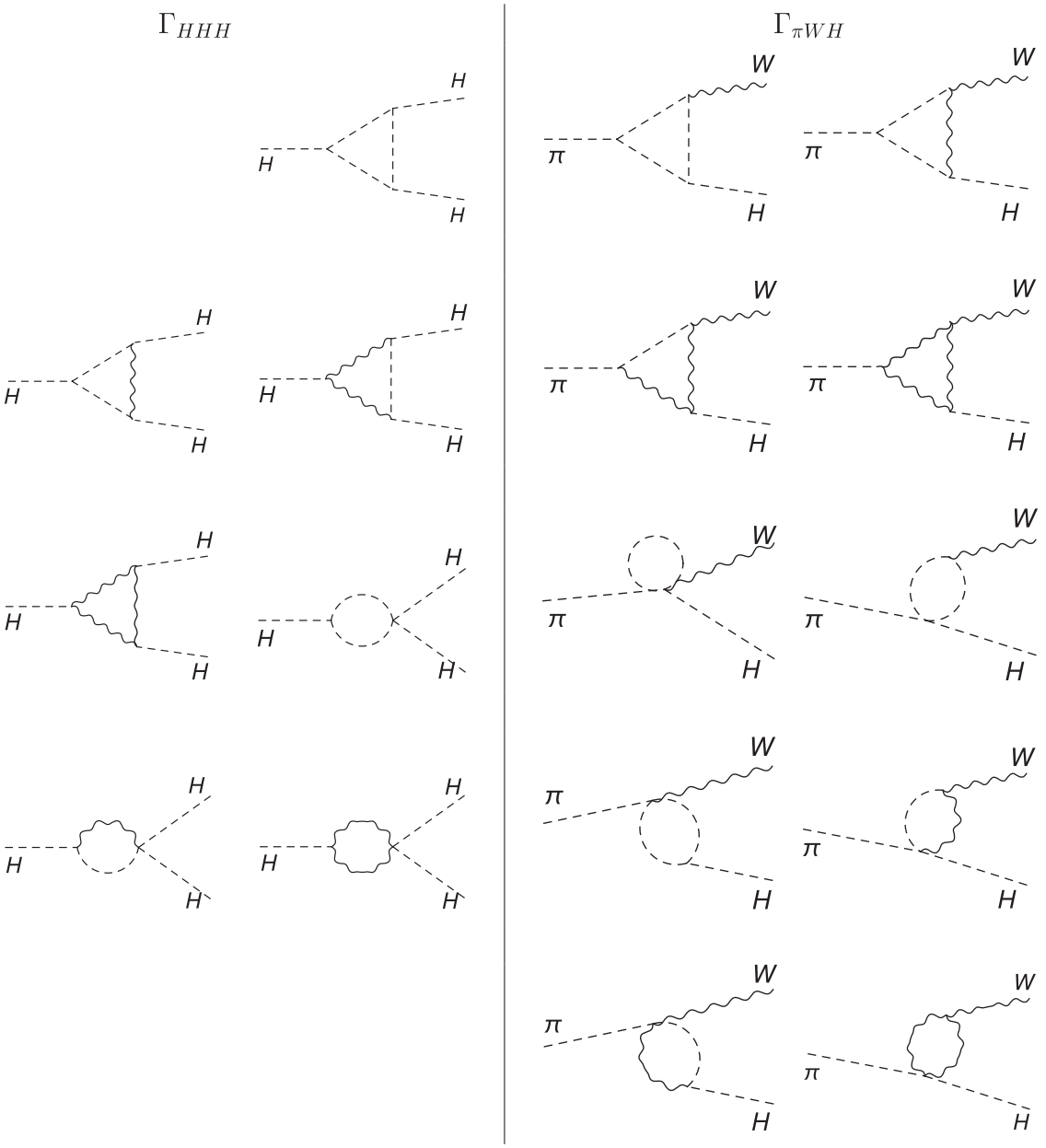

FIG. 6. Generic loop diagrams for the HHH and πWH Green's functions in the EChL. The topologies for AHH and ZHH are the same as for πWH.

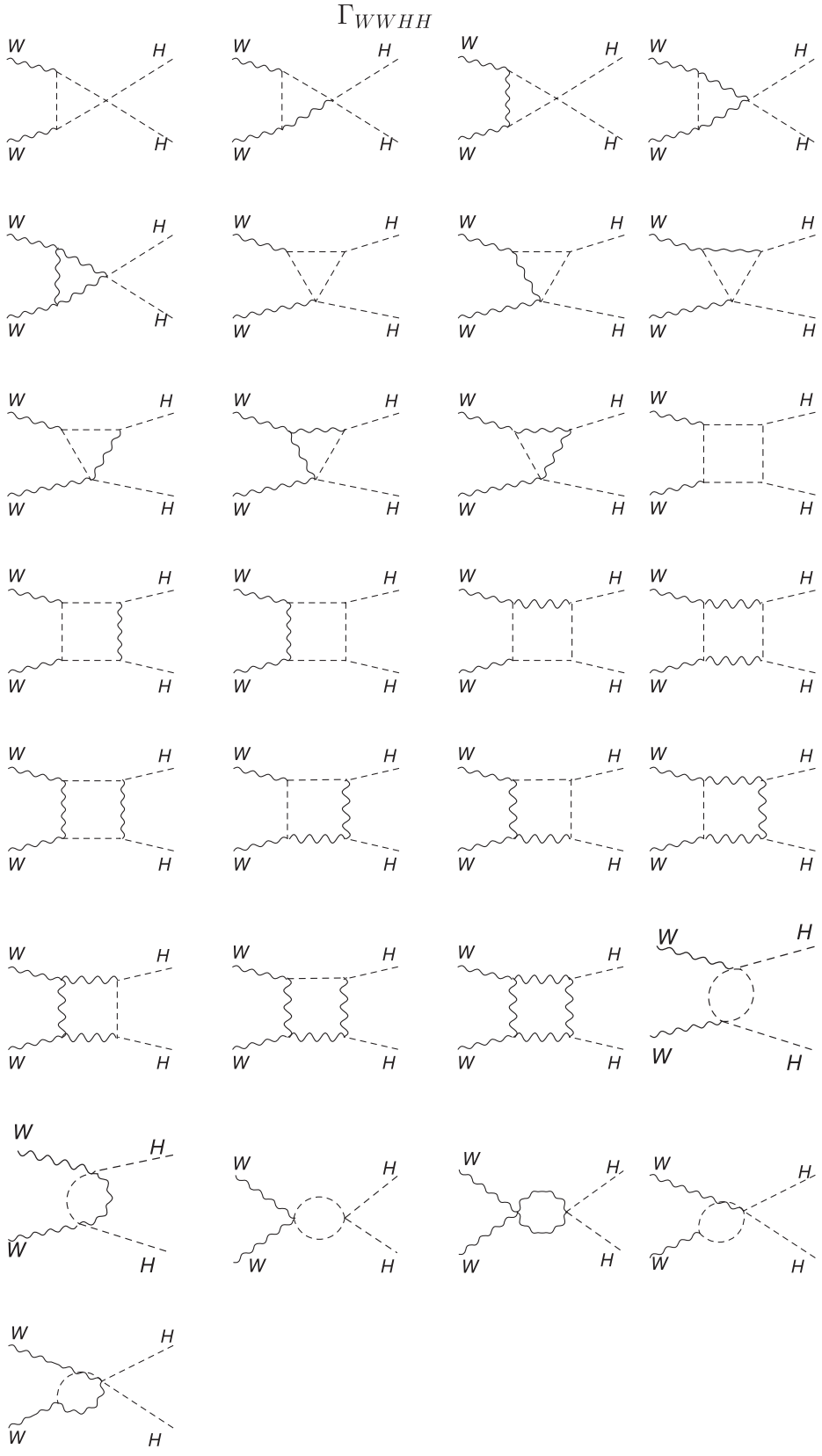

FIG. 7. Generic loop diagrams for the $WWHH$ Green's functions in the EChL.

Regarding the AHH and ZHH Green's functions, they have the same generic topologies as $\Gamma_{\pi WH}$, but they give finite results in both the EChL and SM. We omit the corresponding diagrams for brevity.

Finally, the one-loop diagrams for the $WWHH$ 1PI Green's function are presented in Fig. 7. Also, the results in the EChL depend on a, b, κ_3, and κ_4, and again there is a different (nontrivial) momentum dependence.

[1] I. Brivio and M. Trott, Phys. Rep. **793**, 1 (2019).
[2] A. Dobado and D. Espriu, Prog. Part. Nucl. Phys. **115**, 103813 (2020).
[3] M. J. Herrero and R. A. Morales, Phys. Rev. D **104**, 075013 (2021).
[4] R. L. Delgado, A. Dobado, and F. J. Llanes-Estrada, J. High Energy Phys. 02 (2014) 121.
[5] I. n. Asiáin, D. Espriu, and F. Mescia, Phys. Rev. D **105**, 015009 (2022).
[6] M. B. Gavela, K. Kanshin, P. A. N. Machado, and S. Saa, J. High Energy Phys. 03 (2015) 043.
[7] G. Buchalla, O. Cata, A. Celis, M. Knecht, and C. Krause, Phys. Rev. D **104**, 076005 (2021).
[8] K. Fujikawa, B. Lee, and A. Sanda, Phys. Rev. D **6**, 2923 (1972).
[9] L. Faddeev and V. Popov, Phys. Lett. **25B**, 29 (1967).
[10] I. Brivio, T. Corbett, O. Éboli, M. Gavela, J. Gonzalez-Fraile, M. Gonzalez-Garcia, L. Merlo, and S. Rigolin, J. High Energy Phys. 03 (2014) 024.
[11] D. Domenech, M. J. Herrero, R. A. Morales, and M. Ramos, arXiv:2208.05452.
[12] M. Gonzalez-Lopez, M. J. Herrero, and P. Martinez-Suarez, Eur. Phys. J. C **81**, 260 (2021).
[13] W. R. Inc., Mathematica, Version 10.4, Champaign, IL, 2016.
[14] A. Alloul, N. D. Christensen, C. Degrande, C. Duhr, and B. Fuks, Comput. Phys. Commun. **185**, 2250 (2014).
[15] T. Hahn, Comput. Phys. Commun. **140**, 418 (2001).
[16] T. Hahn and M. Perez-Victoria, Comput. Phys. Commun. **118**, 153 (1999).
[17] V. Shtabovenko, R. Mertig, and F. Orellana, Comput. Phys. Commun. **256**, 107478 (2020).
[18] H. H. Patel, Comput. Phys. Commun. **197**, 276 (2015).
[19] C. G. Bollini and J. J. Giambiagi, Nuovo Cimento B **12**, 20 (1972).
[20] G. 't Hooft and M. Veltman, Nucl. Phys. **B44**, 189 (1972).
[21] F.-K. Guo, P. Ruiz-Femenía, and J. J. Sanz-Cillero, Phys. Rev. D **92**, 074005 (2015).
[22] G. Buchalla, O. Cata, A. Celis, M. Knecht, and C. Krause, Nucl. Phys. **B928**, 93 (2018).
[23] F. A. Dreyer, A. Karlberg, J.-N. Lang, and M. Pellen, Eur. Phys. J. C **80**, 1037 (2020).